Neuron

Article

A role for the cerebellum in motor-triggered alleviation of anxiety

Graphical abstract

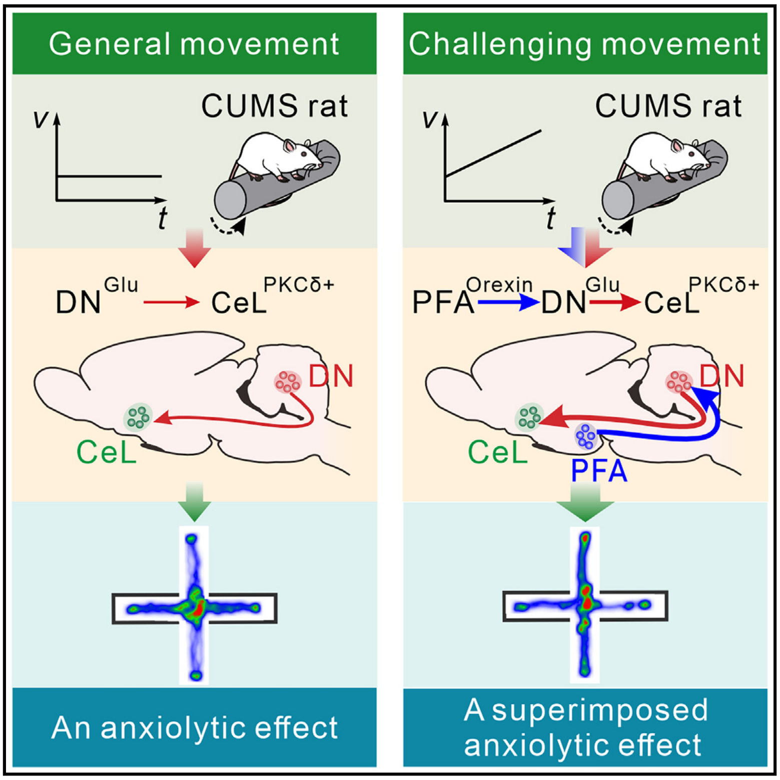

Highlights

- Functional connectivity between cerebellum and amygdala correlated with anxiety
- Cerebellar DN glutamatergic neurons directly innervate and excite CeL PKCδ^+ neurons
- Motor activity activates the cerebello-amygdalar circuit to ameliorate anxiety
- Challenging movement recruits PFA-DN orexinergic projection to drive the DN-CeL circuit

Authors

Xiao-Yang Zhang, Wen-Xia Wu,
Li-Ping Shen, ..., Chris I. De Zeeuw,
Jian-Jun Wang, Jing-Ning Zhu

Correspondence

jnzhu@nju.edu.cn

In brief

The brain mechanisms by which exercise improves mood remain unclear. Zhang et al. dissect a hypothalamo-cerebello-amygdalar circuit bridging the subcortical motor and limbic systems, through which motor activity quickly regulates anxiety at two levels of intensity, and shed light on developing challenging exercise strategies and cerebellar-targeted interventions for anxiety.

Zhang et al., 2024, Neuron *112*, 1–17
April 3, 2024 © 2024 The Author(s). Published by Elsevier Inc.
https://doi.org/10.1016/j.neuron.2024.01.007

CellPress

Please cite this article in press as: Zhang et al., A role for the cerebellum in motor-triggered alleviation of anxiety, Neuron (2024), https://doi.org/10.1016/j.neuron.2024.01.007

Neuron

CellPress

Article

A role for the cerebellum in motor-triggered alleviation of anxiety

Xiao-Yang Zhang,[1,2,10] Wen-Xia Wu,[1,10] Li-Ping Shen,[1,7,10] Miao-Jin Ji,[1,8,10] Peng-Fei Zhao,[4] Lei Yu,[1,9] Jun Yin,[1] Shu-Tao Xie,[1] Yun-Yong Xie,[1] Yang-Xun Zhang,[1] Hong-Zhao Li,[1] Qi-Peng Zhang,[1,2] Chao Yan,[1,3] Fei Wang,[4] Chris I. De Zeeuw,[5,6] Jian-Jun Wang,[1,2] and Jing-Ning Zhu[1,2,3,11,*]

[1]State Key Laboratory of Pharmaceutical Biotechnology, National Resource Center for Mutant Mice, Department of Anesthesiology, Nanjing Drum Tower Hospital, and Department of Physiology, School of Life Sciences, Nanjing University, Nanjing 210023, China
[2]Institute for Brain Sciences, Nanjing University, Nanjing 210023, China
[3]Chemistry and Biomedicine Innovation Center, Nanjing University, Nanjing 210023, China
[4]Early Intervention Unit, Department of Psychiatry, The Affiliated Brain Hospital of Nanjing Medical University, Nanjing 210029, China
[5]Department of Neuroscience, Erasmus MC, 3015 CN Rotterdam, the Netherlands
[6]Netherlands Institute for Neuroscience, 1105 BA Amsterdam, the Netherlands
[7]Department of Neurosurgery, Jiangnan University Medical Center, Wuxi 214002, China
[8]NMPA Key Laboratory for Research and Evaluation of Narcotic and Psychotropic Drugs, School of Anesthesiology, Xuzhou Medical University, Xuzhou 221004, China
[9]Institute of Physical Education, Jiangsu Second Normal University, Nanjing 211200, China
[10]These authors contributed equally
[11]Lead contact
*Correspondence: jnzhu@nju.edu.cn

https://doi.org/10.1016/j.neuron.2024.01.007

SUMMARY

Physical exercise is known to reduce anxiety, but the underlying brain mechanisms remain unclear. Here, we explore a hypothalamo-cerebello-amygdalar circuit that may mediate motor-dependent alleviation of anxiety. This three-neuron loop, in which the cerebellar dentate nucleus takes center stage, bridges the motor system with the emotional system. Subjecting animals to a constant rotarod engages glutamatergic cerebellar dentate neurons that drive PKCδ^+ amygdalar neurons to elicit an anxiolytic effect. Moreover, challenging animals on an accelerated rather than a constant rotarod engages hypothalamic neurons that provide a superimposed anxiolytic effect via an orexinergic projection to the dentate neurons that activate the amygdala. Our findings reveal a cerebello-limbic pathway that may contribute to motor-triggered alleviation of anxiety and that may be optimally exploited during challenging physical exercise.

INTRODUCTION

Coordination of movements and control of emotions are two separate, yet related, functions of the central nervous system (CNS). Motor actions not only constitute an important component and physiological basis for the expression of emotions, but they also improve mental health by reducing negative moods and promoting cognitive function. Indeed, the notion that physical exercise confers protection against anxiety and depression is supported by several prospective cohort studies.[1–3] However, little is known about the neural substrates underlying the interaction of motor control and emotional processing.

The attention to the potential role of the cerebellum in higher functions,[4,5] next to that for sensorimotor coordination,[6,7] has been increasing. Imaging studies reveal a significant activation of the cerebellum during emotional or cognitive processing in healthy subjects[8–11] and highlight aberrant volume, functional connectivity, and spontaneous activity of the cerebellum in patients suffering from anxiety[12] and/or other neuropsychiatric disorders such as depression, autism, and schizophrenia.[13–16] Moreover, patients with focal cerebellar lesions may show a consistent pattern of cognitive and affective deficits, which is termed cerebellar cognitive affective syndrome.[17] However, whereas the cognitive dysfunctions of this syndrome can now be readily explained via cerebellar projections to specific parts of the brainstem, thalamus, and cerebral cortex,[18–24] the cerebellar circuit underlying bidirectional regulation of emotions remains largely enigmatic.[25,26] Given that the limbic system is the central hub for emotional regulation, with the amygdala in a key role for bidirectional control of anxiety,[27–29] we investigated whether and how the cerebellum is connected to the limbic emotional system, and if so, to what extent such a loop provides a neural mechanism that can underlie the alleviation of anxiety by physical exercise.

© 2024 The Author(s). Published by Elsevier Inc.
This is an open access article under the CC BY-NC license (http://creativecommons.org/licenses/by-nc/4.0/).

Please cite this article in press as: Zhang et al., A role for the cerebellum in motor-triggered alleviation of anxiety, Neuron (2024), https://doi.org/10.1016/j.neuron.2024.01.007

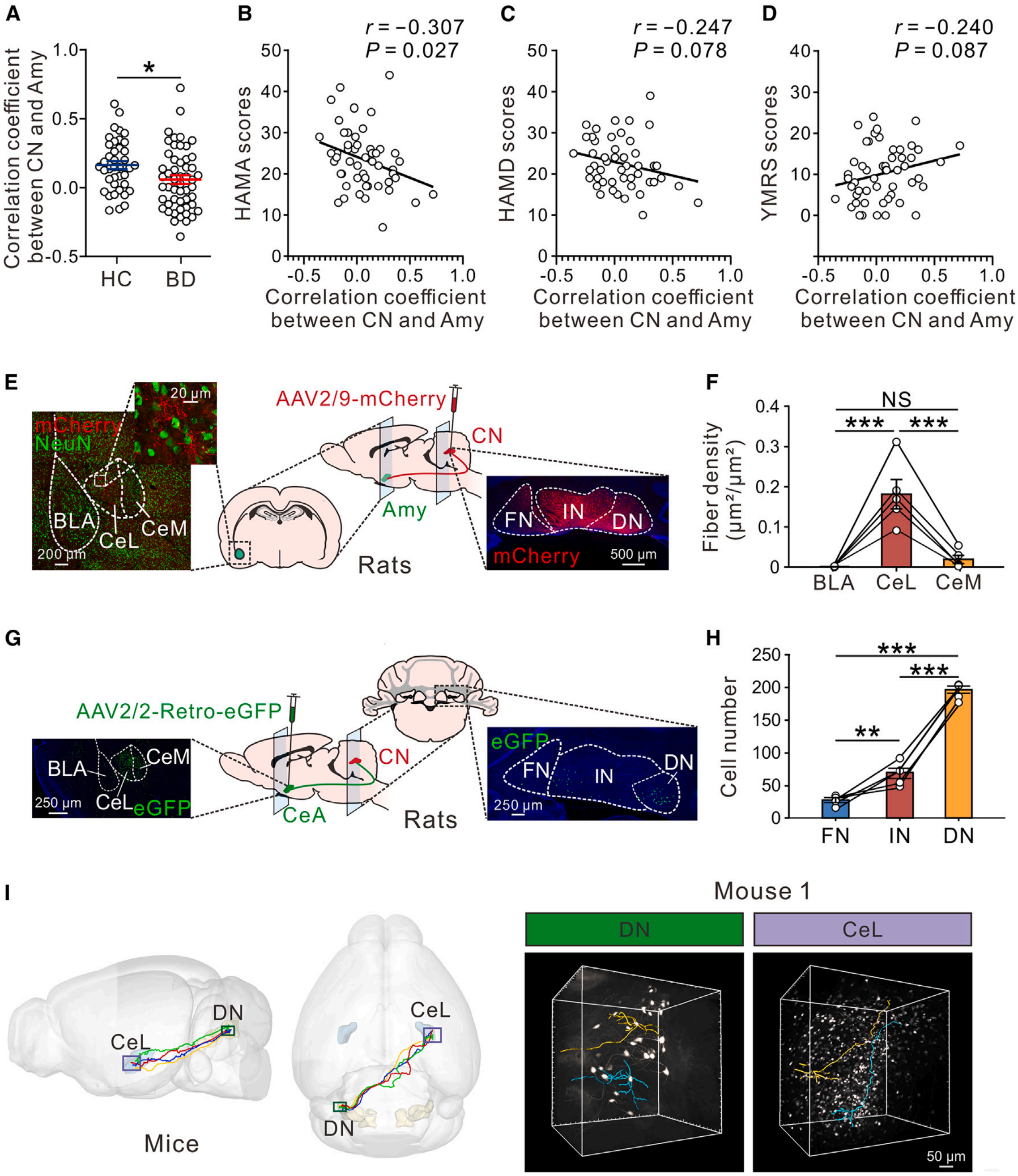

Figure 1. A direct cerebello-amygdalar circuit negatively correlated with anxiety

(A) Cerebellar nuclei (CN)-amygdala (Amy) functional connectivity in patients with bipolar disorder (BD, n = 52) is significantly lower than that in healthy control (HC, n = 40).

(B) A negative correlation between Hamilton Anxiety Rating Scale (HAMA) scores and CN-Amy functional connectivity in patients with BD (n = 52).

(C) There is no significant correlation between Hamilton Depression Rating Scale (HAMD) scores and CN-Amy functional connectivity in patients with BD (n = 52).

(D) There is no significant correlation between Young Mania Rating Scale (YMRS) scores and CN-Amy functional connectivity in patients with BD (n = 52).

(E) Schematics and images of targeting the anterograde viral tracer AAV2/9-hSyn-mCherry to the rat CN, including fastigial (FN), interposed (IN), and dentate (DN) nuclei (right), and anterogradely labeled mCherry-positive fibers in the amygdala, including basolateral (BLA), centrolateral (CeL), and centromedial (CeM) amygdala (left).

(F) Statistics of the density of mCherry-positive fibers in the BLA, CeL, and CeM of rats (n = 5).

(G) Schematic and images of targeting the retrograde viral tracer AAV2/2-Retro-eGFP to the rat central amygdala (CeA, left), including CeL and CeM, and retrogradely labeled eGFP-positive neurons in the FN, IN, and DN (right).

(H) Statistics of the cell number of cerebello-amygdalar projection neurons in the FN, IN, and DN of rats (n = 5).

(legend continued on next page)

RESULTS

A direct cerebello-amygdalar projection and its functional impact on anxiety symptoms

Since anxiety disorders often occur along with other mental illnesses,[30] we collected resting-state functional magnetic resonance imaging (fMRI) data from patients with bipolar disorder (BD), in which anxiety is the most prevalent comorbid diagnosis.[31] Compared with healthy control (HC) subjects, BD patients showed on average lower functional connectivity between the cerebellar nuclei and amygdala (Figure 1A). Pearson correlation analysis revealed that the Hamilton Anxiety Rating Scale (HAMA) score (Figure 1B), but not the Hamilton Depression Rating Scale (HAMD) score (Figure 1C) or Young Mania Rating Scale (YMRS) score (Figure 1D), showed a trend of negative correlation with cerebello-amygdalar functional connectivity in BD patients. Independent from the fact that this correlation between a behavioral and a connectivity score does not allow for any conclusion about the causal or consequential nature of the relation, the trend toward a weaker correlation in BD patients points toward an interaction between two brain regions that may be connected.[32–35]

Because fMRI only enables large-scale, brain-wide mapping of functional connectivity, to find out whether the cerebellum directly projects to the amygdala at cellular and circuit level, we injected the anterograde viral tracer AAV2/9-hSyn-mCherry into the rat cerebellar nuclei (Figures 1E and S1A). The mCherry-positive afferents were distributed mainly in the centrolateral amygdala (CeL) and to a lesser extent in the central medial amygdala, whereas the basolateral amygdala contained virtually no labeled terminals (Figures 1F and S1B). Retrograde tracing with AAV2/2-Retro-eGFP from CeL (Figures 1G and S1C) revealed that most of the cerebellar nuclear neurons projecting to the amygdala were concentrated in the dentate nucleus (DN), which is phylogenetically the youngest cerebellar nucleus,[36] and which is increasingly implicated in emotional control.[8,11,17] In contrast, only few labeled neurons were scattered in the fastigial and interposed nuclei (Figures 1H, S1D, and S1E). Next, we employed trans-monosynaptic retrograde rabies tracing and fluorescence micro-optical sectioning tomography (fMOST) to map the long-range direct afferent projections from DN neurons to CeL neurons at the mesoscopic scale in mice (Figure S2A). The full morphological reconstruction of four DN neurons showed that DN axons can project to the contralateral CeL without collateral axonal branches (Figures 1I and S2B; Video S1). The distribution pattern of DN neurons projecting to the CeL in mice was very similar to that of rats (Figures S2C and S2D), indicating that the cerebello-amygdalar circuit appears well conserved among species.

Motor activity ameliorates anxiety and activates cerebello-amygdalar output

Next, we subjected rats to anxiety assays following rotarod running at a constant speed (10 rpm) for 4 consecutive days to validate the effect of motor exercise on anxiety-like behaviors. Compared with their naive littermates, these rats showed an increased preference for the open arms of the elevated plus maze and the light compartment of the light/dark box, while the total distance traveled was unaffected (Figures 2A and 2B). These data indicate that the locomotion exercise induced a decrease in anxiety level.

To confirm that the relatively sparse cerebello-amygdalar connections are functional during locomotion, we recorded Ca^{2+} activity from CeL neurons *in vivo* using miniature fluorescence microscopy (i.e., visualization of GCaMP7f via an Inscopix miniscope) while rats were running on a rotarod rotating at constant speed (Figure 2C). We found that 73.3% (22/30) of the recorded CeL neurons were activated during rotarod running, which was similar to the percentage (66.6%, 20/30) of CeL neurons activated by optogenetic stimulation of the DN (Figures 2D–2G). Among them, the majority (56.6%) responded to both rotarod running and optogenetic stimulation (Figures 2D–2G; Video S2). To further validate that the activation of CeL neurons during rotarod running was triggered by cerebellar afferent inputs, we studied the impact of optogenetic silencing of the DN-CeL projections on the responses of CeL neurons to running. Inhibitory opsin eNpHR was selectively expressed in DN neurons projecting to CeL in a Cre-dependent manner (Figures S3A and S3B), and opto-inhibition of the DN-CeL pathway significantly suppressed the enhanced Ca^{2+} activity of CeL neurons during rotarod running (Figures S3C–S3G; Video S3). Notably, the percentage of running-sensitive neurons suppressed by opto-inhibition of DN-CeL pathway (27/33, 81.8%; Figures S3D–S3I) is comparable to that of running-sensitive neurons activated by opto-stimulation of DN (17/22, 77.3%). These data indicate that the DN-CeL projections carry exercise-dependent information.

Exercise induces the long-term plasticity of glutamatergic input from DN to CeL to ameliorate anxiety

To investigate whether the rotarod running paradigm that improves anxiety may induce neuroplastic changes in the cerebello-amygdalar circuit, we first further explored our resting-state fMRI data obtained in rats. These data only showed an increased functional connectivity between the cerebellar nuclei and the amygdala, following 4 days of running on a rotarod rotating at a constant speed of 10 rpm (Figures 3A–3C), suggesting an exercise-induced plasticity of the cerebello-amygdalar circuit. Notably, there were no significant changes in the functional connectivity between the cerebellum and other key nodes

---

(I) Sagittal and horizontal views (left panel) demonstrating the axonal morphologies of the 4 DN neurons projecting to CeL in mice, and raw data (right panel) with a volume of 0.5 × 0.5 × 0.5 mm^3 containing 2 DN neurons and their targeting CeL neurons from a mouse brain. The raw data shown in the right panel is corresponding to the DN-CeL circuit shown in yellow and blue in the left panel.

Data are mean ± SEM. Unpaired t test for (A), Pearson correlation coefficient test and simple linear regression for (B)–(D), and one-way ANOVA for (F) and (H). $^{*}p < 0.05$; $^{**}p < 0.01$; $^{***}p < 0.001$; NS, not significant. For statistics, see Table S1.

See also Figures S1 and S2 and Video S1.

Please cite this article in press as: Zhang et al., A role for the cerebellum in motor-triggered alleviation of anxiety, Neuron (2024), https://doi.org/10.1016/j.neuron.2024.01.007

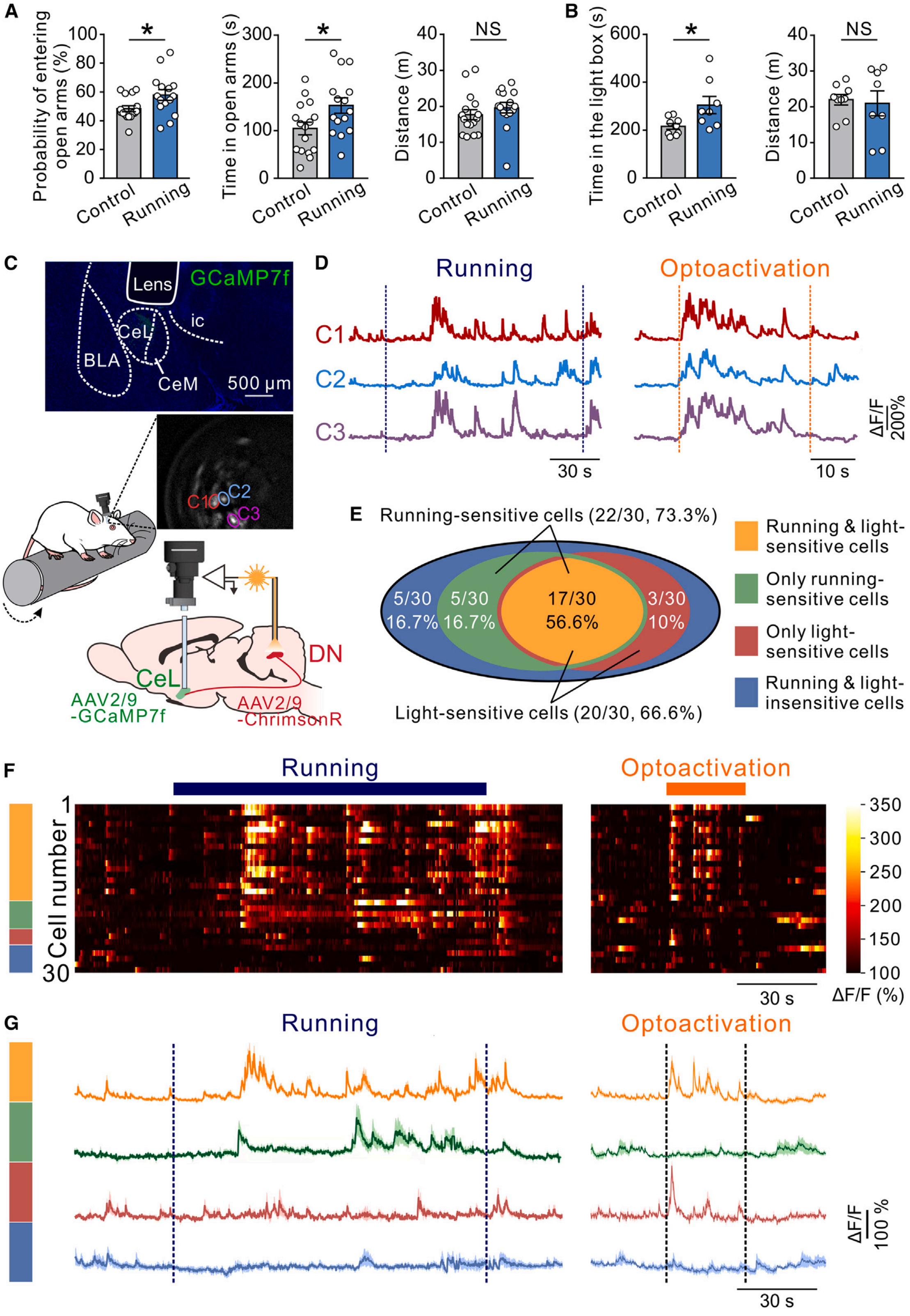

(legend on next page)

of the limbic system,[37,38] except for the one between the amygdala and ventral hippocampus (Figures 3A–3C and S4). Although the cross-species comparison is limited by the fact that animals typically require anesthesia to undergo MRI scanning, these large-scale fMRI data on rats underscore the contribution of the cerebello-amygdalar projection to amelioration of anxiety induced by motor activity.

We next set out to characterize the synaptic output and potential plasticity of the cerebellar input to the amygdala at the cell physiological level. Hereto, we studied the responses of CeL neurons in acute slices from rats that received an injection of AAV2/9-hSyn-ChR2-mCherry into the DN (Figure 3D). Optostimulation of the ChR2-expressing DN afferents evoked fast excitatory postsynaptic currents (EPSCs) in CeL neurons at an average latency of 3.73 ± 0.24 ms (Figure 3F). These EPSCs were mediated by mpact of NBQX (Figure 3E). The optogenetically evoked EPSCs could also be blocked by tetrodotoxin and subsequently be reinstated by administration of 4-aminopyridine (Figure 3G), highlighting the monosynaptic nature of the glutamatergic input from DN fibers onto CeL neurons. Accordingly, the retrograde tracing results showed that the labeled DN neurons projecting to CeL were immunopositive for glutamate (Figures S5A and S5B). Since rotarod running enhanced the cerebello-amygdalar functional connectivity and also exerted an anxiolytic effect, we hypothesized that the activity of afferent inputs from the DN might have induced long-term synaptic plasticity in CeL neurons. As shown in Figures 3D, 3H, and 3I, we microinjected AAV2/9-hSyn-oChIEF-tdTomato into the DN and found that high-frequency optical stimulation of oChIEF-expressing afferent terminals in CeL evoked long-term potentiation (LTP) of EPSCs at DN-CeL synapses. Notably, intracellularly labeled CeL neurons that showed light-induced EPSCs and LTP were all positive for PKCδ (Figure 3J). In addition, Cre-dependent anterograde trans-monosynaptic tracing results (Figures S5C–S5F) further confirmed the direct monosynaptic projection from DN glutamatergic neurons onto CeL PKCδ$^+$ neurons. Since PKCδ$^+$ neurons in the CeL are presumably one of the major cell types controlling anxiolytic processes,[39–41] these data suggest that cerebellar DN afferents may exert anxiolytic effects by modulating PKCδ$^+$ CeL neurons.

To find out whether the glutamatergic DN-CeL inputs could influence anxiety-like behaviors, we injected AAV2/9-CaMKII-ChR2-mCherry into the DN of rats and subsequently studied the impact of optogenetic activation of DN glutamatergic terminals within CeL (Figure 3K). This stimulation significantly ameliorated anxiety-like behaviors in the elevated plus maze (Figure 3L) and concomitantly increased c-Fos expression specifically in PKCδ$^+$ CeL neurons (Figures S5G–S5J). Likewise, selectively activating the DN neurons projecting to the CeL (DN^{CeL}) with an intraperitoneal/intra-CeL injection of clozapine-N-oxide (CNO) following Cre-dependent expression of the excitatory hM3Dq designer receptor exclusively activated by a designer drug (DREADD) also significantly reduced anxiety-like behaviors (Figures S5K and S5L). Moreover, both the optogenetic (Figure 3L) and chemogenetic (Figures S5K and S5L) activation had no impact on the distance the rats traveled in the elevated plus maze, indicating that the DN-CeL circuit is not involved in the regulation of locomotor activity per se. To find out whether chemogenetic suppression of the glutamatergic DN-CeL pathway could prevent the anxiolytic effects induced by rotarod running, we next selectively expressed the inhibitory hM4Di DREADD in DN^{CeL} glutamatergic neurons, using Cre-dependent retrograde AAV vector, and microinjected CNO for 4 consecutive days intraperitoneally or intra-CeL before daily rotarod running (Figure 3M). As shown in Figure 3N, the anxiolytic effect of rotarod running was indeed eliminated, without any change in locomotor activity, suggesting that alleviation of anxiety by exercise can be controlled in a bidirectional fashion by the glutamatergic DN neurons projecting to the PKCδ$^+$ neurons in CeL.

Orexinergic hypothalamo-cerebellar projection is engaged during challenging exercises

As different motor paradigms may have different effects on mood, we next compared the effects of constant and accelerating rotarod running on chronic unpredictable mild stress (CUMS)-induced anxiety in rats. Running on a rotarod rotating for 4 days at a constant speed (10 rpm) induced a moderate, yet significant, increase in open-arm time and open-arm entries as well as time spent in the light box in our CUMS anxiety assays. However, running on a rotarod rotating with an acceleration of 0.2 rpm/s, a more challenging form of exercise,[42] significantly enhanced these outcome measures of stress, as compared with the outcomes following the constant rotarod paradigm (Figures 4A–4C).

As the neuropeptide orexin facilitates motor challenges[42] as well as stress resilience,[43,44] we next evaluated whether the

Figure 2. Rotarod running produces anxiolytic-like behaviors and activates CeL neurons receiving direct inputs from cerebellar DN

(A and B) A 4-day constant rotarod running (10 rpm) induces anxiolytic-like behaviors but does not influence locomotor activity in the elevated plus maze test (A; n = 16 rats for control; n = 15 rats for running) and light/dark box test (B; n = 9 rats for control; n = 8 rats for running) in rats.

(C) Schematic of GCaMP7f and ChrimsonR virus infusions in the centrolateral amygdala (CeL) and cerebellar dentate nucleus (DN), respectively (lower panel), and microendoscopic calcium imaging in the CeL (middle panel), using a miniscope combined with a GRIN lens, during rotarod running or opto-activation of DN neurons. The upper panel shows an image of GCaMP7f expression (green) and GRIN lens location in CeL. BLA, basolateral amygdala; CeM, centromedial amygdala; ic, internal capsule.

(D) Calcium traces from 3 CeL neurons that were activated by both rotarod running and DN optostimulation.

(E) Proportions of CeL neurons sensitive/insensitive to constant rotarod running (10 rpm) and/or DN opto-activation (n = 30 cells, from 3 rats).

(F) Heatmaps of normalized ΔF/F traces illustrating the four types of response kinetics (indicated by orange, green, red, and blue) of CeL neurons to rotarod running and DN opto-activation (n = 30 cells, from 3 rats).

(G) Averaged calcium traces of the CeL neurons were sensitive to both running and light (orange), only running (green), only light (red), or to neither running nor light (blue).

Data are mean ± SEM. Unpaired t test for (A) and (B). *$p < 0.05$; NS, not significant. For statistics, see Table S1.

See also Figure S3 and Videos S2 and S3.

Please cite this article in press as: Zhang et al., A role for the cerebellum in motor-triggered alleviation of anxiety, Neuron (2024), https://doi.org/10.1016/j.neuron.2024.01.007

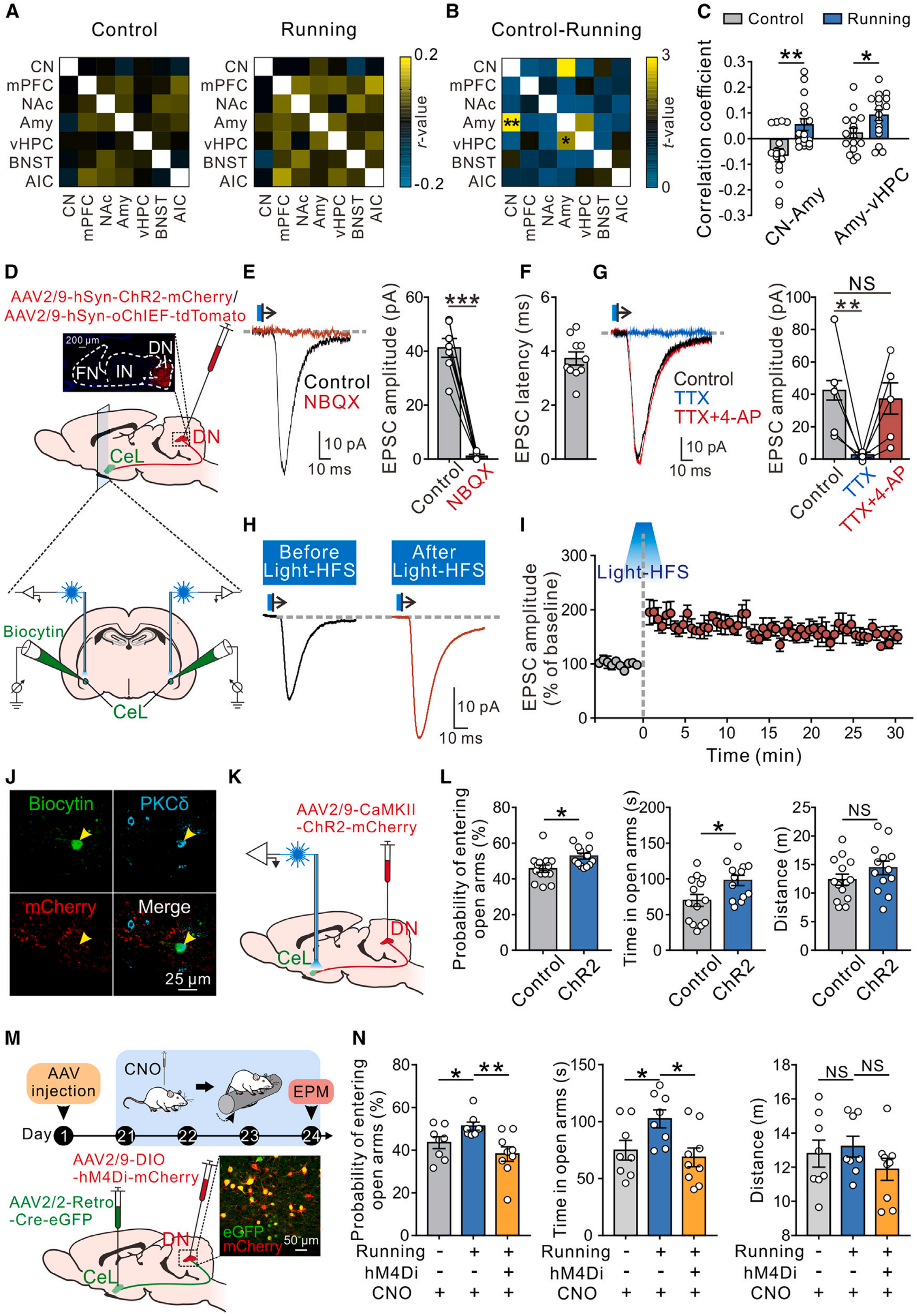

(legend on next page)

Please cite this article in press as: Zhang et al., A role for the cerebellum in motor-triggered alleviation of anxiety, Neuron (2024), https://doi.org/10.1016/j.neuron.2024.01.007

hypothalamic orexinergic fibers that are known to project to the DN[45] participate in the amelioration effects of rotarod running on CUMS-induced anxiety. Retrograde tracing from DN to the hypothalamus combined with orexin and c-Fos immunostaining revealed that orexinergic DN-projecting neurons in the perifornical area (PFA) of the hypothalamus, the predominant source of orexin in the brain,[46–48] are indeed remarkably activated by the challenging, but not the constant, rotarod task (Figure 4D). Accordingly, our ELISA results showed that accelerating, but not constant, rotarod running induced a significant elevation of orexin levels in the DN (Figure 4E). Considering that the PFA also sends direct orexinergic fibers to the amygdala,[49] we determined whether the PFA orexinergic projections to the amygdala are also activated. Intriguingly, PFA orexinergic neurons projecting to CeL were neither activated by constant nor by accelerating rotarod running (Figure 4F). Moreover, the levels of orexin the PFA fibers released into the CeL were not increased during exercise (Figure 4G). Furthermore, we found that the PFA orexinergic neurons that directly project to CeL are not part of the same group that projects to DN (Figures 4H–4J). All these results render the involvement of direct PFA-CeL orexinergic projection in the alleviation of anxiety by motor activity less likely.

Next, we generated a new transgenic rat line expressing Cre recombinase driven by the orexin promoter so as to manipulate the hypothalamo-cerebellar orexinergic projection with cell-type-specific optogenetics and chemogenetics (for use of Rosa26-tdTomato reporter to determine validation of the orexin-Cre rat line, see Figures 5A and 5B). Notably, ChR2 was Cre-dependently expressed by PFA orexinergic neurons in orexin-Cre rats (Figure 5C). As predicted, optogenetic activation of orexinergic PFA terminals within the cerebellar DN remarkably improved the CUMS-induced anxiety (Figure 5D). We next infected orexinergic PFA neurons projecting to DN (PFA^{DN}) in a retrograde direction in orexin-Cre rats, following injection of AAV2/2-Retro-DIO-hM4Di-eGFP in DN, so as to be able to induce chemogenetic inhibition (Figure 5E). Selective chemogenetic inhibition of PFA orexinergic afferents in DN significantly suppressed the alleviation of anxiety-like behaviors of CUMS orexin-Cre rats, induced by the challenging rotarod exercise (Figure 5F). Additionally, pharmacological blockage (Figures 5G and 5H) or genetic knockdown (Figures 5I–5K) of orexin 2 receptors, which mediate the orexin-evoked excitation of DN neurons,[50] also eliminated the anxiolytic effects of the challenging exercise. Together, these results suggest that the orexinergic hypothalamo-cerebellar pathway may play a critical role in the amelioration of CUMS-induced anxiety by a challenging exercise.

Hypothalamo-cerebello-amygdalar circuit involved in anxiety alleviation is a cascade of excitatory signaling

To test the synaptic nature of the orexinergic hypothalamic fibers onto DN neurons, we made whole-cell patch-clamp recordings in cerebellar slices. Bath application of orexin-A, one of the splice variants of orexin, excited glutamatergic projection neurons in the DN but had no impact on the activities of GABAergic neurons and interneurons in the DN (Figures 6A, 6B, and S6A–S6E). Pharmacological blockage with selective blockers of ion channels/exchangers combined with the ramp command test showed that the excitatory postsynaptic effect (Figure S6F) of orexin-A on DN glutamatergic neurons was mediated by both activation of Na^{+}-Ca^{2+} exchangers and the closure of inward rectifier potassium channels (Figures 6C and S6G–S6J).

Since PFA^{DN} orexinergic neurons were significantly activated when an animal was facing severe motor challenges (Figure 4D), we wanted to evaluate whether the effects of manipulation of the orexinergic afferents to DN neurons, especially to DN^{CeL}

Figure 3. Monosynaptic projections from DN glutamatergic neurons to CeL PKCδ^{+} neurons have long-term plasticity and mediate the improvement of anxiety by locomotion

(A) Correlation matrices derived from global resting-state fMRI signal analysis across anxiety-related brain regions and cerebellar nuclei (CN) in control (n = 16 rats) and running groups (n = 17 rats) of rats. Amy, amygdala; AIC, anterior insular cortex; BNST, bed nucleus of the stria terminalis; mPFC, medial prefrontal cortex; NAc, nucleus accumbens; vHPC, ventral hippocampus.

(B) Difference in functional connectivity between control (n = 16 rats) and rotarod running groups (n = 17 rats).

(C) Enhancement of functional connectivity between CN and Amy as well as Amy and vHPC (n = 16 rats for control; n = 17 rats for running).

(D) Schematic of optogenetic manipulations of DN nucleofugal terminals following ChR2/oChIEF virus infusion in DN (inset) and whole-cell patch-clamp recordings of CeL neurons with biocytin-containing pipettes in brain slices.

(E) Bath application of AMPA receptor antagonist NBQX totally blocked the EPSCs evoked by opto-activation of ChR2-expressing DN nucleofugal terminals (n = 7 cells, from 4 rats).

(F) Onset latency of light-evoked EPSCs that were recorded in CeL neurons (n = 10 cells, from 5 rats).

(G) Light-evoked EPSCs were blocked by tetrodotoxin (TTX) and reappeared after the application of TTX plus 4-aminopyridine (4-AP) (n = 5 cells, from 4 rats).

(H and I) High-frequency optogenetic stimulation (Light-HFS) of oChIEF-expressing DN nucleofugal terminals in CeL induced long-term potentiation (LTP) of EPSCs at DN-CeL synapse (n = 8 cells, from 3 rats).

(J) Confocal images of one of the light-responsive CeL neurons triple-labeled with biocytin (green), PKCδ (cyan), and ChR2-mCherry (red); the neuron is indicated by yellow arrowheads.

(K and L) Optogenetic activation of the DN-CeL glutamatergic terminals following CaMKII-ChR2 virus infusion in DN reduced anxiety-like behaviors rather than locomotor activity in the elevated plus maze (n =14 rats for control; n = 13 rats for ChR2).

(M) Scheme of Retro-Cre and Cre-inducible hM4Di virus infusions in CeL and DN (inset, double-labeled neurons) as well as CNO injections, and subsequent studies on their impact on rotarod running induced anxiolytic-like behaviors in the elevated plus maze (EPM).

(N) Chemogenetic inhibition of the DN-CeL glutamatergic projections blocked the improvement of anxiety-like behaviors by rotarod running (n = 8 rats for running−/hM4Di−/CNO+; n = 8 rats for running+/hM4Di−/CNO+; n = 9 rats for running+/hM4Di+/CNO+).

Data are mean ± SEM. Unpaired t test for (C), (L), and (N); paired t test for (E); and RM one-way ANOVA for (G). $^{*}p < 0.05$; $^{**}p < 0.01$; $^{***}p < 0.001$; NS, not significant. For statistics, see Table S1.

See also Figures S4 and S5.

Please cite this article in press as: Zhang et al., A role for the cerebellum in motor-triggered alleviation of anxiety, Neuron (2024), https://doi.org/10.1016/j.neuron.2024.01.007

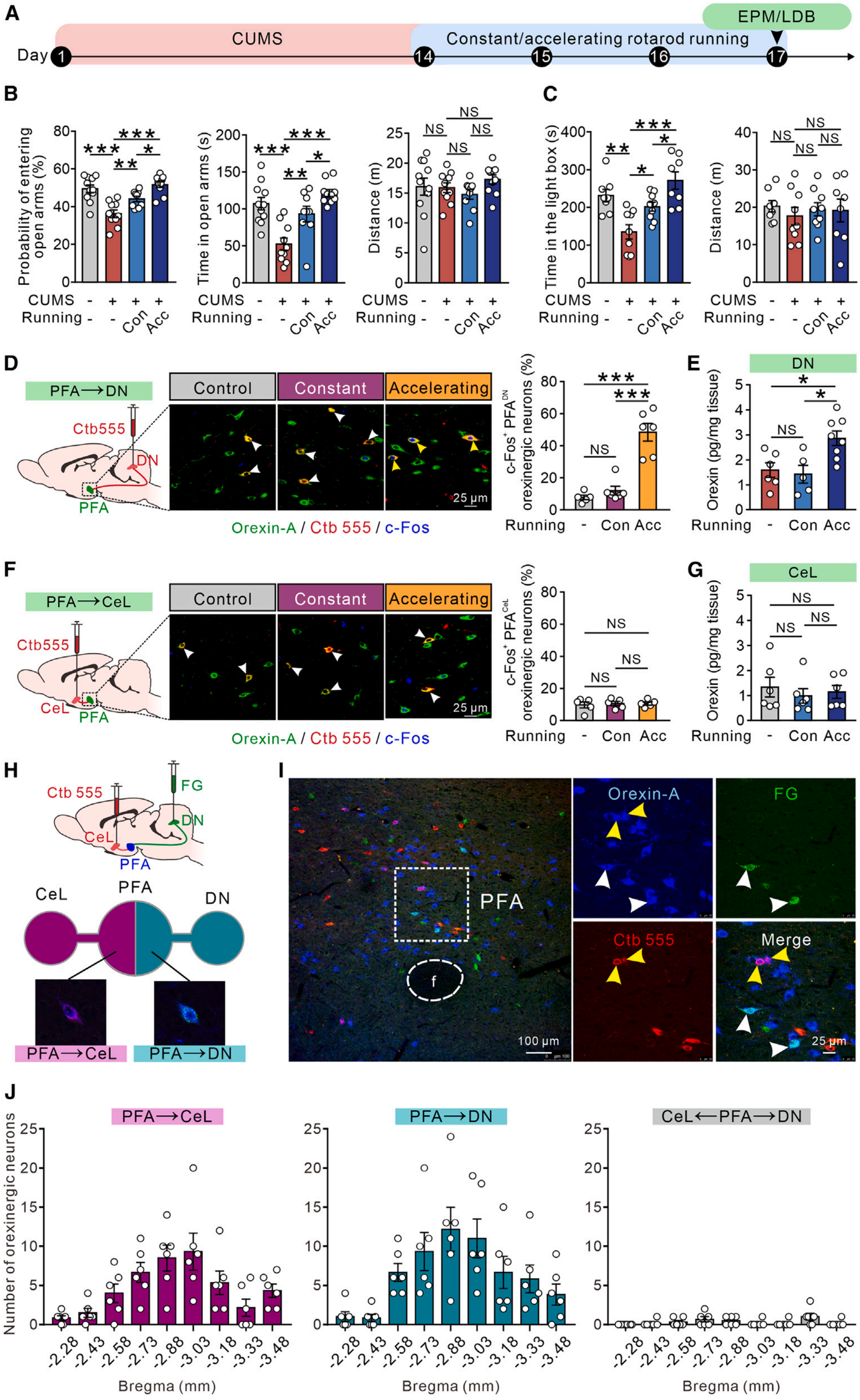

(legend on next page)

neurons, on their spiking activity during running were in line with these findings. As shown in Figure 6D, we thereto expressed eNpHR-mCherry and ChR2-eYFP in a Cre-dependent fashion in PFA orexinergic neurons and DN^{CeL} neurons in orexin-Cre rats, respectively. With this approach we were able to identify increasing spiking activity of cerebellar DN^{CeL} neurons expressing ChR2, following activation with blue light (Figure 6D). Vice versa, opto-inhibition of PFA-DN orexinergic afferent terminals expressing eNpHR-mCherry by yellow light indeed suppressed the DN^{CeL} neuronal firing rates. Notably, these effects were particularly prominent during accelerating, rather than constant, rotarod running (Figures 6E and 6F). Moreover, *in vivo* multichannel recordings showed that microinjection of the selective orexin 2 receptor antagonist TCS-OX2-29 into the DN blocked the hypothalamic orexinergic input significantly and selectively in that the increased firing rate of DN neurons during accelerating rotarod running was diminished, whereas that during constant rotarod running was not (Figures S7A–S7C).

Along the same vein, running on an accelerating rotarod induced a stronger c-Fos expression in most CeL $PKC\delta^+$ neurons (whether some activated $PKC\delta^-$ neurons were inhibitory interneurons or other neurons needs further investigation) in CUMS rats than running on a constantly rotating rotarod, and the neuronal activation induced by challenging, but not regular, movements could be blocked by pharmacological inhibition of the orexinergic inputs to DN neurons (Figures S7D and S7E). Accordingly, general chemogenetic inhibition of the DN-CeL projection nearly totally blocked the anxiolytic effect of the challenging exercise (Figures S7F–S7H), while specific chemogenetic inhibition of the DN glutamatergic neurons expressing Flp-dependent hM4Di-mCherry that are directly innervated by the PFA orexinergic neurons and directly project to CeL $PKC\delta^+$ neurons effectively blocked anxiety amelioration induced by selective optostimulation of PFA-DN orexinergic afferent terminals expressing Cre-inducible ChR2-eYFP in CUMS orexin-Cre rats (Figures 6G and 6H). In conjunction, these results suggest that challenging exercise can effectively alleviate stress-induced anxiety via activation of the orexin-driven hypothalamo-cerebello-amygdalar (PFA-DN-CeL) circuit.

Increasing the motor challenge to optimize the ameliorating impact on anxiety

The data highlighted above raise the question of the extent to which the level of motor challenge can be optimized to alleviate the maximum amount of anxiety. As shown in Figure 7A, we thereto explored the anxiolytic effects of exercise at different levels of challenge in CUMS rats. Rotarod running with accelerations of 0.12, 0.2, and 0.4 rpm/s showed increasingly stronger amelioration effects on anxiety-related behaviors (Figure 7B), indicating that the challenge level may be an essential parameter to consider when applying exercise therapy for anxiety. Given that increasing the exercise challenge improved anxiety in a virtual linear fashion, we next determined to what extent the cerebellar nuclei may form potentially an effective central target for applying brain stimulation to ameliorate anxiety (Figure 7C). We thereto used integrated opto-electrodes for simultaneous optostimulation and multichannel recordings of cerebellar DN^{CeL} glutamatergic neurons expressing oChIEF, which allows for measuring reliable responses to sustained high-frequency optostimulation, while investigating the effect of motor challenge on anxiety (Figure 7D). We found that optostimulation of DN^{CeL} neurons at 60 Hz, which simulated DN neuronal firing rate during animals running on an accelerating (0.2 rpm/s) rotarod, alleviated the anxiety of CUMS rats more effectively than optostimulation at 30 Hz (Figures 7E and 7F), which mimicked DN neuronal firing frequency during running on a constant (10 rpm) rotarod. These effects occurred concomitantly with increases in firing rate of DN^{CeL} neurons, indicating that activation of DN^{CeL} glutamatergic neurons may ameliorate anxiety in CUMS rats in a frequency-dependent manner. Taken together, these results suggest that

Figure 4. Challenging movements activate PFA-DN, but not PFA-CeL orexinergic projections

(A) Scheme for evaluating the effect of constant and accelerating rotarod running on anxiety-like behaviors in CUMS-induced rats in the elevated plus maze (EPM) and light/dark box (LDB).

(B and C) Accelerating rotarod running (Acc, acceleration of 0.2 rpm/s) improved anxiety-like behaviors more significantly than constant rotarod running (Con, 10 rpm) in EPM (B; n = 11 rats for CUMS−/running−; n = 10 rats for CUMS+/running−; n = 9 rats for CUMS+/Con; n = 10 rats for CUMS+/Acc) and LDB (C; n = 8 rats for CUMS−/running−; n = 9 CUMS+/running−; n = 9 rats for CUMS+/Con; n = 8 rats for CUMS+/Acc). In contrast, locomotion distance was unaffected.

(D) Images of the c-Fos staining (blue) in PFA orexinergic (green) neurons projecting to DN (red) before (n = 5 rats) and following constant (10 rpm, n = 6 rats) or accelerating (0.2 rpm/s, n = 6 rats) rotarod running. Yellow arrowheads indicate the Ctb555 retrogradely labeled PFA^{DN} orexinergic neurons with c-Fos expression, whereas white arrowheads indicate c-Fos-negative PFA^{DN} orexinergic neurons. Statistics show that accelerating, but not constant, rotarod running activated PFA^{DN} orexinergic neurons.

(E) ELISA analyses showed that orexin levels in DN were significantly increased after accelerating rotarod running (n = 8 tissue samples, from 24 rats) as compared with control (n = 6 tissue samples, from 18 rats) or constant rotarod running (n = 5 tissue samples, from 15 rats).

(F) Images of the c-Fos staining (blue) in PFA orexinergic (green) neurons projecting to CeL (red) before (n = 5 rats) and following constant (10 rpm, n = 5 rats) or accelerating (0.2 rpm/s, n = 5 rats) rotarod running. White arrowheads indicate c-Fos-negative PFA^{CeL} orexinergic neurons. Statistics showed that neither constant nor accelerating rotarod running activated PFA^{CeL} orexinergic neurons.

(G) ELISA analyses showed that orexin levels in CeL have no significant difference among control (n = 6 tissue samples, from 18 rats), constant (n = 6 tissue samples, from 18 rats), and accelerating rotarod running (n = 6 tissue samples, from 18 rats).

(H) Schematic of microinjecting Fluoro-Gold (FG) into DN and Ctb-555 into CeL to retrogradely label PFA^{DN} and PFA^{CeL} orexinergic neurons, respectively. The PFA orexinergic neurons that project to CeL show dual labeling (purple) of Ctb-555 (red) and orexin-A (blue), while those that project to DN show dual labeling (cyan) of FG (green) and orexin-A (blue).

(I) The retrograde labeled PFA orexinergic neurons projecting to CeL and to DN barely overlap.

(J) Statistics of distribution of PFA orexinergic neurons that project to CeL only, to DN only, and to both along the anterior-posterior axis of the hypothalamus; it should be noted that the numbers reflect the total number of labeled cells observed in the six rats involved.

Data are mean ± SEM. Unpaired t test combined with one-way ANOVA for (B) and (C) and one-way ANOVA for (D)–(G). $^*p < 0.05$; $^{**}p < 0.01$; $^{***}p < 0.001$; NS, not significant. For statistics, see Table S1.

Please cite this article in press as: Zhang et al., A role for the cerebellum in motor-triggered alleviation of anxiety, Neuron (2024), https://doi.org/10.1016/j.neuron.2024.01.007

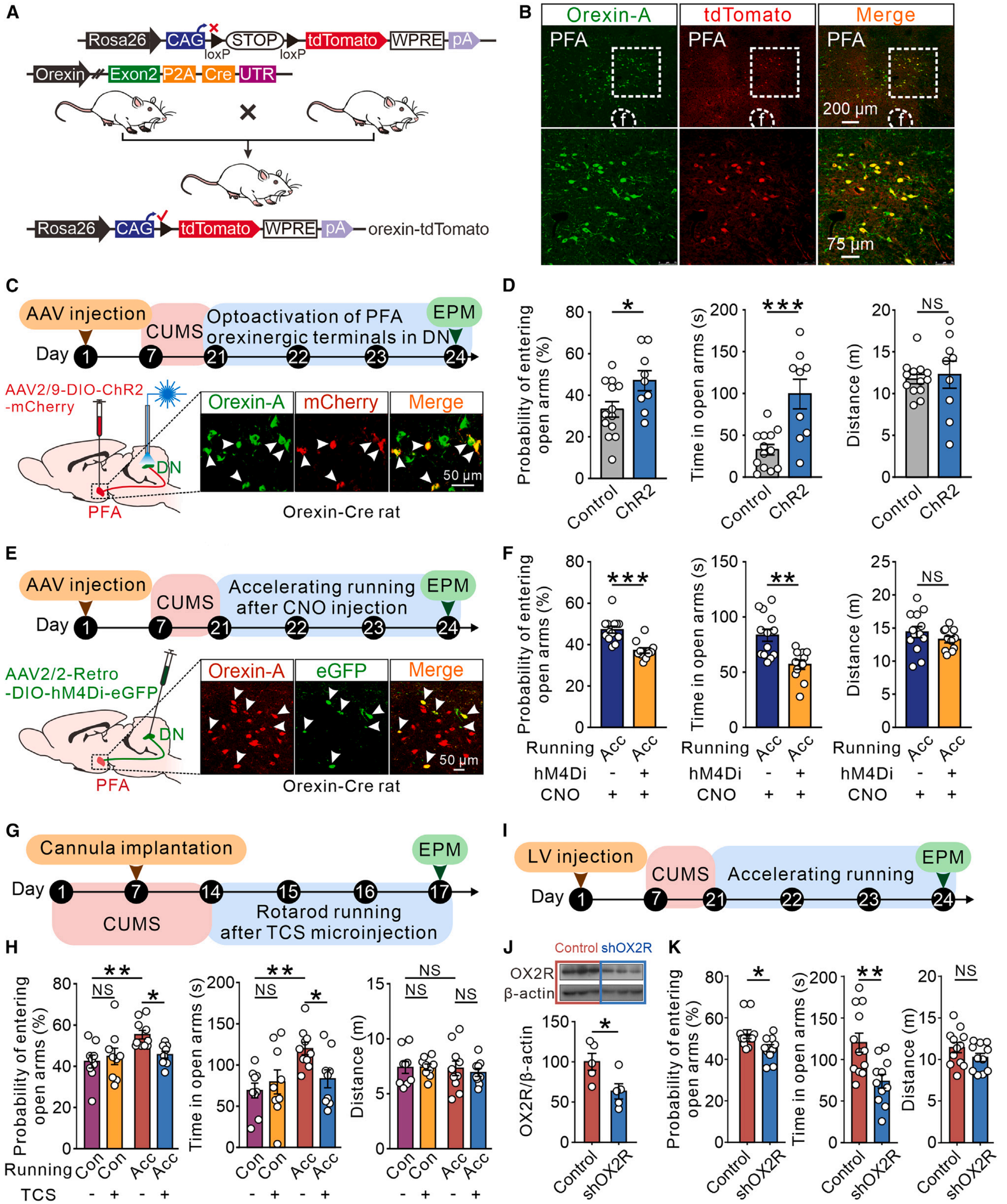

Figure 5. Challenging movements ameliorate stress-induced anxiety via activation of PFA-DN orexinergic projections

(A) Schematic of generation of orexin-Cre::tdTomato rats.

(B) Confocal image of tdTomato (red) and immunofluorescence labeling for orexin-A (green) in the perifornical area (PFA) in orexin-Cre::tdTomato rats.

(legend continued on next page)

Please cite this article in press as: Zhang et al., A role for the cerebellum in motor-triggered alleviation of anxiety, Neuron (2024), https://doi.org/10.1016/j.neuron.2024.01.007

challenging exercise and manipulation of the cerebellum might form an effective intervention strategy for anxiety.

DISCUSSION

Alleviation of anxiety by motor activity forms an integral part of our daily life; whether going for a walk to refresh our mind or running excessively in the park to recuperate from a stressful event, we are all well aware of the beneficial impact.[1,51] Yet, apart from some general interactions between the periphery of our body and our CNS,[52,53] it has remained unclear which mechanisms inside our brain underlie this process of motor-dependent anxiolysis. Here, we shed light on the potential contribution of a three-neuron loop in which the cerebellar DN takes center stage. Regular locomotion activates glutamatergic DN neurons projecting to PKCδ^+ neurons in the CeL, from which anxiolytic processes can be coordinated.[27] More challenging forms of exercise recruits an additional pathway, originating in the orexinergic neurons in the PFA of the hypothalamus that provide excitation of the DN neurons on top of the regular activation. Thus, the hypothalamo-cerebello-amygdalar circuit may exert its effects at two levels of intensity, operating like an engine with multiple transitions.

The connections between the cerebellum and limbic system have attracted much attention, but a direct cerebello-limbic functional circuitry has thus far not been elucidated. Based on extracellular recordings of evoked potentials *in vivo* and traditional staining of degenerated fibers and terminals in cats and monkeys, Heath and Harper[54] suggested already almost half a century ago that the cerebellar fastigial nucleus may project to the basal lateral amygdala. Other studies, however, have argued that the connections between the cerebellum and limbic system, including the amygdala, are indirect, probably relaying signals via a multisynaptic pathway involving the thalamic nuclei and/or ventral tegmental area.[26,55] Using trans-monosynaptic viral anterograde and retrograde tracing, fMOST, patch-clamp and multichannel recordings, as well as optogenetic and chemogenetic manipulation, we reveal here for the first time a monosynaptic projection from the cerebellar nuclei to the amygdala, in particular the CeL, in rats and mice. Although the fastigial nucleus and interposed nucleus also appear to send some axons directly to the CeL, the majority of cerebello-amgydalar fibers originate from the phylogenetically younger DN. Interestingly, the DN^{CeL} neurons also receive direct innervation and modulation from PFA orexinergic neurons. This three-neuron loop thereby directly bridges the cerebellar motor system with the limbic emotional system at both the input level, i.e., the hypothalamus, and the output level, i.e., the amygdala. This raises the possibility that increased processing in the hypothalamus under stressful conditions exerts a dampening homeostatic effect onto the amygdala via the cerebellum, provided that sufficient physical exercise is taking place. Our fMRI data suggest that this loop is one of the main contributors to mediate exercise-dependent alleviation of anxiety. However, we cannot exclude that other loops also contribute. For example, functional hyperconnectivity between the DN and cerebral cortex has been suggested to affect anxiety disorders in adolescents.[12] Likewise, one could imagine that challenging motor tasks that require intense planning will activate the prefrontal cortex[19,21,56,57] and thereby also affect anxiolytic processes in the amygdala.[28,29] Moreover, how the effects are actually integrated within the network of the amygdala and whether and to what extent inhibitory interneurons or other neurons downstream of the DN^{CeL} neurons within this network are actively involved or not remain to be uncovered.

The increasing evidence for widespread connections between cerebellum and non-motor structures, including the direct cerebello-amygdalar circuit, advances our understanding of the fine structural and functional modules of the cerebellum in that they highlight that olivocerebellar modules do not only facilitate sensorimotor coordination and cognition but also more autonomic and affective functions, including emotions like anxiety. In fact, each cerebellar micromodule appears to be tailored to generate outputs with a specific functional profile.[25] Since the amygdala also plays a prominent role in many other forms of emotional behavior, including, for example, sexual drive and aggression,[58–60] further elucidation of the functions of this cerebello-amygdalar circuit in such behaviors may well provide more detailed insight into the affective functions of the various specific DN micromodules.

The question remains as to how changes in the hypothalamo-cerebello-amygdalar circuit are implicated in psychiatric or neurological diseases. In the current study, we showed that in patients suffering from anxiety control, such as those diagnosed with BD, the functional connectivity between the cerebellum and amygdala appears to be negatively correlated with the severity of the anxiety symptoms. One may find similar changes in functional connectivity in the hypothalamo-cerebello-amygdalar circuit in diseases characterized by deficits in motor control, such

---

(C) Schematic of Cre-dependent virus ChR2 infusions in PFA in orexin-Cre rats, CUMS, opto-activation of PFA orexinergic terminals in DN, and EPM. Orexinergic neurons with ChR2 expression in PFA are indicated with white arrowheads.

(D) Opto-activation of PFA orexinergic terminals in DN significantly improved CUMS-induced anxiety (n = 13 rats for control; n = 9 rats for ChR2).

(E) Scheme for infusion of Cre-inducible AAV2/2-Retro-DIO-hM4Di virus in DN of orexin-Cre rats, CUMS, rotarod running after CNO injection, and EPM. Orexinergic neurons in PFA projecting to DN in CUMS-induced orexin-Cre rats are indicated with white arrowheads.

(F) Chemogenetic inhibition of PFA-DN orexinergic projections suppressed the improvement of CUMS-induced anxiety by accelerating rotarod running (n = 13 rats for Acc/hM4Di−/CNO+; n = 11 rats for Acc/hM4Di+/CNO+).

(G and H) Intra-DN microinjection of TCS-OX2-29 (TCS), a selective orexin 2 receptor (OX2R) antagonist, eliminated the specific anxiolytic effect of accelerating (0.2 rpm/s) rotarod running (n = 9 rats for constant + saline; n = 9 rats for constant + TCS; n = 10 rats for accelerating + saline; n = 9 rats for accelerating + TCS).

(I) Scheme of genetic knockdown of OX2Rs with shOX2R lentivirus, CUMS, accelerating running, and EPM.

(J) Identification of the downregulation efficiency of OX2R protein by western blot (n = 5 tissue samples from 15 rats for each group).

(K) Knockdown of OX2R in DN reduced the amelioration of the CUMS-induced anxiety by accelerating rotarod running, while it did not significantly affect the distance traveled (n = 12 rats for control; n = 11 rats for shOXR2).

Data are mean ± SEM. Unpaired t test for (D), (F), (J), and (K) and two-way ANOVA for (H). $^*p < 0.05$; $^{**}p < 0.01$; $^{***}p < 0.001$; NS, not significant. For statistics, see Table S1.

Please cite this article in press as: Zhang et al., A role for the cerebellum in motor-triggered alleviation of anxiety, Neuron (2024), https://doi.org/10.1016/j.neuron.2024.01.007

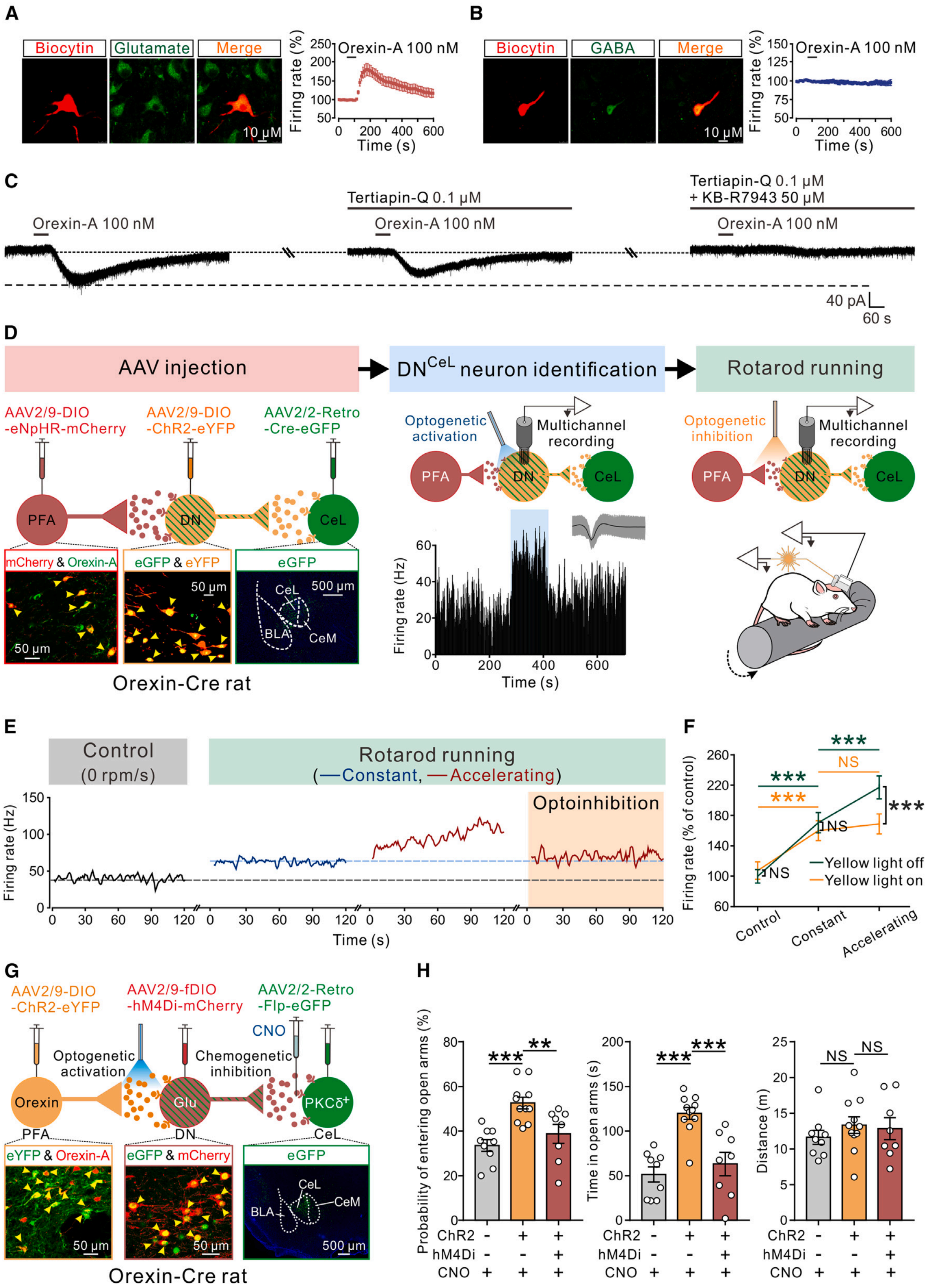

(legend on next page)

Please cite this article in press as: Zhang et al., A role for the cerebellum in motor-triggered alleviation of anxiety, Neuron (2024), https://doi.org/10.1016/j.neuron.2024.01.007

as Parkinson's disease or cerebellar ataxias. For example, aberrations in the functional connectivity of this pathway might contribute to abnormal regulation of emotion and mood in these diseases.[12,61–63] Via similar mechanisms, impairments in functioning of the hypothalamo-cerebello-amygdalar circuit presented here may contribute to the cerebellar cognitive affective syndrome described by Schmahmann and Sherman.[17] In fact, the concurrence of motor and emotional dysfunctions in both Parkinson's disease and cerebellar cognitive affective syndrome, together with our findings on mood improvement by motor activity, points toward the significance of integration of motor and emotional processes, which has been relatively neglected for some time. The hypothalamo-cerebello-amygdalar circuit we reveal in the present study may provide a direct mechanism through which an orchestrated and coordinated behavioral response with integration of motor activity and emotional state is rapidly generated to adapt to the changes in the internal and external environments. Moreover, our current findings on the role of the endogenous orexinergic hypothalamic neurons exerting a strong excitatory response in the DN neurons during motor-dependent anxiolysis by affecting Na^+-Ca^{2+} exchangers and inward rectifier potassium channels may not only provide potential targets for the prevention and intervention of anxiety in related motor disorders, but they also shed light on developing more effective movement prescriptions for anxiety and mood disorders in general, such as high-intensity interval training (HIIT) or vigorous intermittent lifestyle physical activity (VILPA).[64] Indeed, akin recent developments in the treatment of neurological diseases like epilepsy and dystonia,[65–67] directly or indirectly targeting the proper neurons of the cerebellar nuclei, may provide a novel strategy for both invasive and non-invasive forms of interventions to alleviate anxiety.

STAR★METHODS

Detailed methods are provided in the online version of this paper and include the following:

- KEY RESOURCES TABLE
- RESOURCE AVAILABILITY
  - Lead contact
  - Materials availability
  - Data and code availability
- EXPERIMENTAL MODEL AND SUBJECT DETAILS
  - Animals
  - Human subjects
- METHOD DETAILS
  - Resting-state functional magnetic resonance imaging (fMRI)
  - Stereotaxic surgery
  - Anatomical tracing
  - Fluorescence Micro-optical Sectioning Tomography (fMOST)
  - Immunohistochemistry
  - Miniscope Ca^{2+} imaging in freely moving rats
  - Optogenetic and chemogenetic manipulation
  - Behavioral tests
  - Patch-clamp recordings in brain slices
  - Multielectrode array recordings *in vivo*
  - Enzyme-linked immunosorbent assay (ELISA)
  - Western blot
- QUANTIFICATION AND STATISTICAL ANALYSIS

SUPPLEMENTAL INFORMATION

Supplemental information can be found online at https://doi.org/10.1016/j.neuron.2024.01.007.

ACKNOWLEDGMENTS

This work was supported by STI2030-Major Projects-2021ZD0202805 from the Ministry of Science and Technology of China; grants 32030044, 31961160724, 32171012, 12227808, 81725005, U20A6005, and 81671107 from the National Natural Science Foundation of China; grant BK20190008 from the Natural Science Foundation of Jiangsu Province, China; grant 020814380164 from the Fundamental Research Funds for the Central Universities, China; grant 824.02.001 from the Netherlands Organization for Scientific

Figure 6. The orexin-mediated superimposed activation of DN-CeL circuitry contributes to the better anxiolytic effects of challenging exercise

(A and B) Application of orexin-A increased the firing rate of glutamatergic projection neurons (n = 5 cells from 5 rats) in DN but not that of GABAergic neurons or interneurons (n = 5 cells from 5 rats). The glutamatergic (left) or GABAergic (right) nature of the neurons was identified following cellular labeling with biocytin; the orexin-responsive glutamatergic neurons have a relatively large cell body (diameter of 23.24 ± 1.12 μm; n = 5 cells from 5 rats), whereas the GABAergic neurons tend to be smaller (diameter of 7.19 ± 0.32 μm; n = 5 cells from 5 rats).

(C) The orexin-induced inward current in DN glutamatergic projection neurons was partly blocked by tertiapin-Q, a selective blocker for inward rectifier K^+ channels, and totally abolished by combined application of tertiapin-Q and KB-R7943, a selective blocker of Na^+/Ca^{2+} exchanger.

(D) Schematic of Cre-inducible eNpHR (mCherry), Cre-dependent ChR2 (eYFP), and Retro-Cre (eGFP) viral expression in PFA, DN, and CeL, respectively, (left panel) in orexin-Cre rats. Blue light-sensitive neurons recorded in DN are identified as DN^{CeL} neurons (middle panel). Responses of DN^{CeL} neurons to rotarod running and opto-inhibition of PFA orexinergic inputs in DN were recorded and assessed (right panel).

(E) Firing rates of a recorded DN^{CeL} neuron in response to standing on a stationary rotarod, running on a constant (10 rpm) or accelerating (0.2 rpm/s) rotarod, as well as running on an accelerating (0.2 rpm/s) rotarod with opto-inhibition of orexinergic inputs in DN.

(F) Opto-inhibition of orexinergic inputs in DN significantly suppressed the increase in firing rates of DN^{CeL} neurons (n = 27 cells from 4 rats) during accelerating (0.2 rpm/s) but not constant (10 rpm) rotarod running.

(G) Schematic of Cre-inducible ChR2 (eYFP), Flp-dependent hM4Di (mCherry), and Retro-Flp (eGFP) virus infusions in PFA, DN and CeL, respectively, in CUMS-induced orexin-Cre rats. Note that with this strategy, we are able to specifically manipulate activity in the PFA-DN-CeL circuit.

(H) Chemogenetic inhibition of the DN-CeL glutamatergic pathway blocked the anxiolytic-like behaviors induced by optogenetic activation of the PFA-DN orexinergic terminals in the CUSM-induced orexin-Cre rats in the elevated plus maze (n = 9 rats for ChR2-/hM4Di−/CNO+; n = 11 rats for ChR2+/hM4Di−/CNO+; n = 8 rats for ChR2+/hM4Di+/CNO+).

Data are mean ± SEM. RM two-way ANOVA for (F) and unpaired t test for (H). $^{**}p < 0.01$; $^{***}p < 0.001$; NS, not significant. For statistics, see Table S1.

See also Figures S6 and S7.

Please cite this article in press as: Zhang et al., A role for the cerebellum in motor-triggered alleviation of anxiety, Neuron (2024), https://doi.org/10.1016/j.neuron.2024.01.007

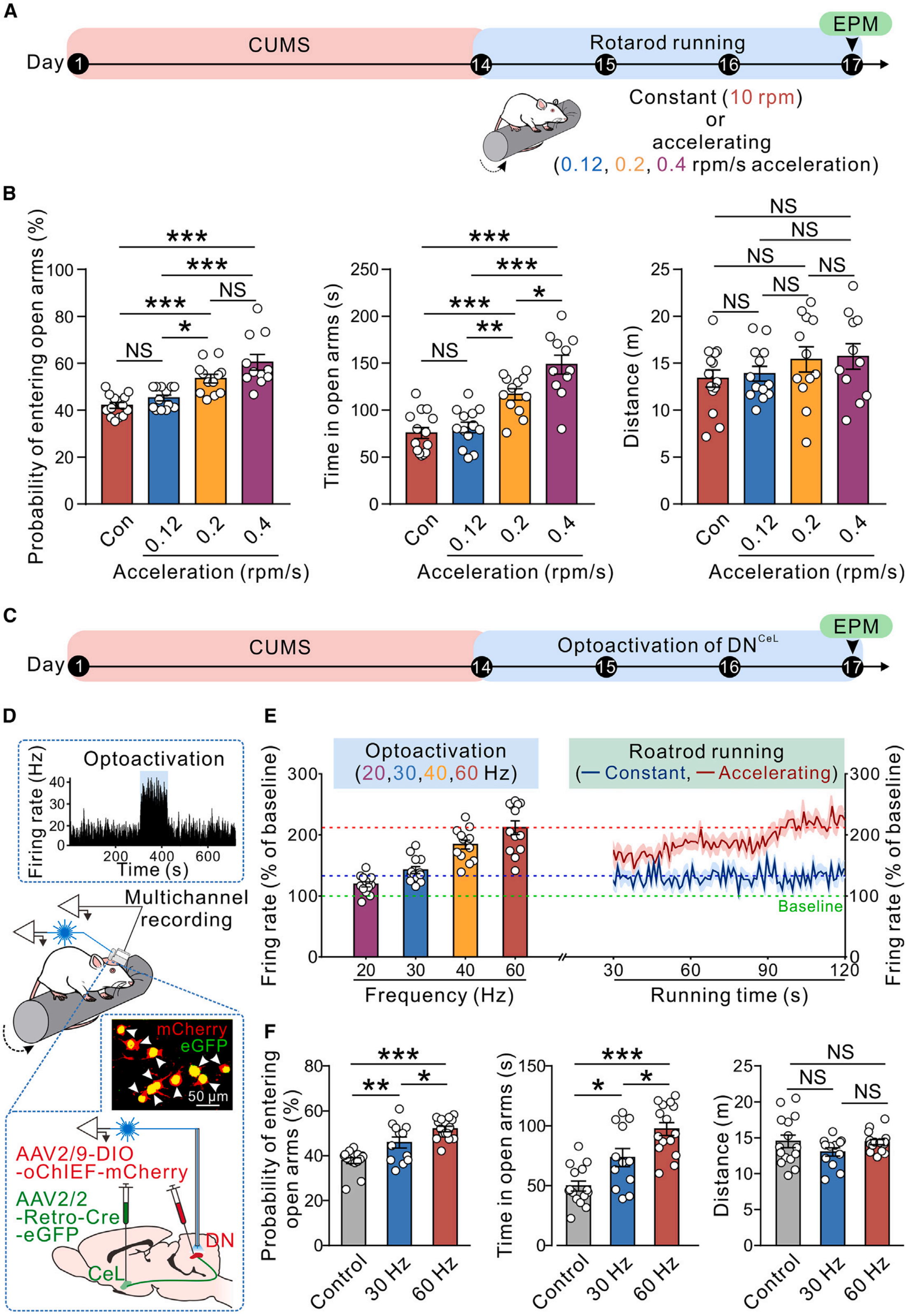

(legend on next page)

Research (NWO-ALW); grant 91120067 from the Netherlands Organization for Medical Sciences (ZonMW); grant 01092019-31082023 from the Medical Neuro-Delta (MD); Gravitation grant DBI2 (NWO); grant TTW/00798883 INTENSE from LSH-NWO; and grant NIN-01CDZ Vriendenfonds (KNAW).

AUTHOR CONTRIBUTIONS

J.-N.Z. conceived and designed the study. X.-Y.Z., W.-X.W., L.-P.S., and M.-J.J. performed all experiments, analyzed data, and prepared figures with contributions from P.-F.Z., L.Y., J.Y., S.-T.X., Y.-Y.X., Y.-X.Z., H.-Z.L., and Q.-P.Z. J.-N.Z., X.-Y.Z., C.I.D.Z., and J.-J.W. interpreted the results and wrote the paper with input from Q.-P.Z., F.W., and C.Y. J.-N.Z. and C.I.D.Z. supervised the project.

DECLARATION OF INTERESTS

The authors declare no competing interests.

Received: September 29, 2022
Revised: March 16, 2023
Accepted: January 5, 2024
Published: January 31, 2024

REFERENCES

1. Noakes, T., and Spedding, M. (2012). Olympics: Run for your life. Nature *487*, 295–296.
2. Kandola, A., Lewis, G., Osborn, D.P.J., Stubbs, B., and Hayes, J.F. (2020). Depressive symptoms and objectively measured physical activity and sedentary behaviour throughout adolescence: a prospective cohort study. Lancet Psychiatry *7*, 262–271.
3. Henriksson, M., Wall, A., Nyberg, J., Adiels, M., Lundin, K., Bergh, Y., Eggertsen, R., Danielsson, L., Kuhn, H.G., Westerlund, M., et al. (2022). Effects of exercise on symptoms of anxiety in primary care patients: A randomized controlled trial. J. Affect. Disord. *297*, 26–34.
4. Zhu, J.N., Yung, W.H., Kwok-Chong Chow, B., Chan, Y.S., and Wang, J.J. (2006). The cerebellar-hypothalamic circuits: potential pathways underlying cerebellar involvement in somatic-visceral integration. Brain Res. Rev. *52*, 93–106.
5. Schmahmann, J.D., Guell, X., Stoodley, C.J., and Halko, M.A. (2019). The Theory and Neuroscience of Cerebellar Cognition. Annu. Rev. Neurosci. *42*, 337–364.
6. Rochefort, C., Arabo, A., André, M., Poucet, B., Save, E., and Rondi-Reig, L. (2011). Cerebellum shapes hippocampal spatial code. Science *334*, 385–389.
7. Romano, V., Zhai, P., van der Horst, A., Mazza, R., Jacobs, T., Bauer, S., Wang, X., White, J.J., and De Zeeuw, C.I. (2022). Olivocerebellar control of movement symmetry. Curr. Biol. *32*, 654–670.e4.
8. Reiman, E.M., Lane, R.D., Ahern, G.L., Schwartz, G.E., Davidson, R.J., Friston, K.J., Yun, L.S., and Chen, K. (1997). Neuroanatomical correlates of externally and internally generated human emotion. Am. J. Psychiatry *154*, 918–925.
9. Allen, G., Buxton, R.B., Wong, E.C., and Courchesne, E. (1997). Attentional activation of the cerebellum independent of motor involvement. Science *275*, 1940–1943.
10. Singer, T., Seymour, B., O'Doherty, J., Kaube, H., Dolan, R.J., and Frith, C.D. (2004). Empathy for pain involves the affective but not sensory components of pain. Science *303*, 1157–1162.
11. Schraa-Tam, C.K., Rietdijk, W.J., Verbeke, W.J., Dietvorst, R.C., van den Berg, W.E., Bagozzi, R.P., and De Zeeuw, C.I. (2012). fMRI activities in the emotional cerebellum: a preference for negative stimuli and goal-directed behavior. Cerebellum *11*, 233–245.
12. Lee, Y.J., Guell, X., Hubbard, N.A., Siless, V., Frosch, I.R., Goncalves, M., Lo, N., Nair, A., Ghosh, S.S., Hofmann, S.G., et al. (2021). Functional alterations in cerebellar functional connectivity in anxiety disorders. Cerebellum *20*, 392–401.
13. Courchesne, E., Yeung-Courchesne, R., Press, G.A., Hesselink, J.R., and Jernigan, T.L. (1988). Hypoplasia of cerebellar vermal lobules VI and VII in autism. N. Engl. J. Med. *318*, 1349–1354.
14. Coesmans, M., Röder, C.H., Smit, A.E., Koekkoek, S.K., De Zeeuw, C.I., Frens, M.A., and van der Geest, J.N. (2014). Cerebellar motor learning deficits in medicated and medication-free men with recent-onset schizophrenia. J. Psychiatry Neurosci. *39*, E3–E11.
15. Bogoian, H.R., King, T.Z., Turner, J.A., Semmel, E.S., and Dotson, V.M. (2020). Linking depressive symptom dimensions to cerebellar subregion volumes in later life. Transl. Psychiatry *10*, 201.
16. Cheng, C., Dong, D., Jiang, Y., Ming, Q., Zhong, X., Sun, X., Xiong, G., Gao, Y., and Yao, S. (2019). State-Related Alterations of Spontaneous Neural Activity in Current and Remitted Depression Revealed by Resting-State fMRI. Front. Psychol. *10*, 245.
17. Schmahmann, J.D., and Sherman, J.C. (1998). The cerebellar cognitive affective syndrome. Brain *121*, 561–579.
18. Wagner, M.J., Kim, T.H., Savall, J., Schnitzer, M.J., and Luo, L. (2017). Cerebellar granule cells encode the expectation of reward. Nature *544*, 96–100.
19. Gao, Z., Davis, C., Thomas, A.M., Economo, M.N., Abrego, A.M., Svoboda, K., De Zeeuw, C.I., and Li, N. (2018). A cortico-cerebellar loop for motor planning. Nature *563*, 113–116.
20. Carta, I., Chen, C.H., Schott, A.L., Dorizan, S., and Khodakhah, K. (2019). Cerebellar modulation of the reward circuitry and social behavior. Science *363*, eaav0581.
21. Chabrol, F.P., Blot, A., and Mrsic-Flogel, T.D. (2019). Cerebellar contribution to preparatory activity in motor neocortex. Neuron *103*, 506–519.e4. e504.
22. Wagner, M.J., Kim, T.H., Kadmon, J., Nguyen, N.D., Ganguli, S., Schnitzer, M.J., and Luo, L. (2019). Shared cortex-cerebellum dynamics in the execution and learning of a motor task. Cell *177*, 669–682.e24.

Figure 7. Challenge exercise and cerebellar optostimulation ameliorate stress-induced anxiety degree-dependently

(A) Scheme of CUMS, rotarod running (at a constant speed of 10 rpm or an acceleration of 0.12, 0.2, or 0.4 rpm/s), and evaluation in the elevated plus maze (EPM).
(B) The amelioration of the CUMS-induced anxiety-like behaviors by running on the constant (n = 14 rats) and accelerating rotarod. The effect increased as the acceleration increased from 0.12 (n = 13 rats) and 0.2 (n = 12 rats) to 0.4 rpm/s (n = 11 rats), while the distance traveled in the EPM was not significantly affected.
(C) Scheme of CUMS, opto-activation of DN^{CeL} neurons, and evaluation in the elevated plus maze (EPM).
(D) Schematic for optogenetic activation of cerebellar DN^{CeL} neurons with Cre-dependent oChIEF (lower panel), as well as multichannel recording of responses of DN^{CeL} neurons to optogenetic stimulation (upper panel) and rotarod running (middle panel) with integrated opto-electrodes.
(E) Increases in firing rates of DN^{CeL} neurons in response to opto-activation at 20, 30, 40, and 60 Hz (histogram in the left, n = 13 cells from 6 rats), as well as constant (10 rpm, blue line, n = 21 cells from 6 rats) and accelerating (acceleration of 0.2 rpm/s, red line, n = 20 cells from 6 rats) rotarod running. Note that optostimulation of DN^{CeL} neurons at 30 and 60 Hz mimicked the firing rates during constant (blue dashed line) and accelerating (red dashed line) rotarod running, respectively.
(F) Opto-activation of DN^{CeL} neurons at 60 Hz produced a stronger anxiolytic effect in CUMS rats than 30 Hz (n = 15 rats for control; n = 12 rats for 30 Hz; n = 15 rats for 60 Hz).
Data are mean ± SEM. One-way ANOVA for (B) and (F). *$p < 0.05$; **$p < 0.01$; ***$p < 0.001$; NS, not significant. For statistics, see Table S1.

Please cite this article in press as: Zhang et al., A role for the cerebellum in motor-triggered alleviation of anxiety, Neuron (2024), https://doi.org/10.1016/j.neuron.2024.01.007

23. Kostadinov, D., and Häusser, M. (2022). Reward signals in the cerebellum: Origins, targets, and functional implications. Neuron *110*, 1290–1303.

24. Bina, L., Romano, V., Hoogland, T.M., Bosman, L.W.J., and De Zeeuw, C.I. (2021). Purkinje cells translate subjective salience into readiness to act and choice performance. Cell Rep. *37*, 110116.

25. De Zeeuw, C.I. (2021). Bidirectional learning in upbound and downbound microzones of the cerebellum. Nat. Rev. Neurosci. *22*, 92–110.

26. Apps, R., and Strata, P. (2015). Neuronal circuits for fear and anxiety - the missing link. Nat. Rev. Neurosci. *16*, 642.

27. Tye, K.M., Prakash, R., Kim, S.Y., Fenno, L.E., Grosenick, L., Zarabi, H., Thompson, K.R., Gradinaru, V., Ramakrishnan, C., and Deisseroth, K. (2011). Amygdala circuitry mediating reversible and bidirectional control of anxiety. Nature *471*, 358–362.

28. Adhikari, A., Lerner, T.N., Finkelstein, J., Pak, S., Jennings, J.H., Davidson, T.J., Ferenczi, E., Gunaydin, L.A., Mirzabekov, J.J., Ye, L., et al. (2015). Basomedial amygdala mediates top-down control of anxiety and fear. Nature *527*, 179–185.

29. Zhu, L., Zheng, D., Li, R., Shen, C.J., Cai, R., Lyu, C., Tang, B., Sun, H., Wang, X., Ding, Y., et al. (2023). Induction of Anxiety-Like Phenotypes by Knockdown of Cannabinoid Type-1 Receptors in the Amygdala of Marmosets. Neurosci. Bull. *39*, 1669–1682.

30. Hyman, S.E. (2019). New Evidence for Shared Risk Architecture of Mental Disorders. JAMA Psychiatry *76*, 235–236.

31. Pavlova, B., Perlis, R.H., Alda, M., and Uher, R. (2015). Lifetime prevalence of anxiety disorders in people with bipolar disorder: a systematic review and meta-analysis. Lancet Psychiatry *2*, 710–717.

32. Jarcho, J.M., Davis, M.M., Shechner, T., Degnan, K.A., Henderson, H.A., Stoddard, J., Fox, N.A., Leibenluft, E., Pine, D.S., and Nelson, E.E. (2016). Early-Childhood Social Reticence Predicts Brain Function in Preadolescent Youths During Distinct Forms of Peer Evaluation. Psychol. Sci. *27*, 821–835.

33. Lee, J., Lee, D., Namkoong, K., and Jung, Y.C. (2020). Aberrant posterior superior temporal sulcus functional connectivity and executive dysfunction in adolescents with internet gaming disorder. J. Behav. Addict. *9*, 589–597.

34. Rosen, A.C., Bhat, J.V., Cardenas, V.A., Ehrlich, T.J., Horwege, A.M., Mathalon, D.H., Roach, B.J., Glover, G.H., Badran, B.W., Forman, S.D., et al. (2021). Targeting location relates to treatment response in active but not sham rTMS stimulation. Brain Stimul. *14*, 703–709.

35. Zito, G.A., Tarrano, C., Jegatheesan, P., Ekmen, A., Béranger, B., Rebsamen, M., Hubsch, C., Sangla, S., Bonnet, C., Delorme, C., et al. (2022). Somatotopy of cervical dystonia in motor-cerebellar networks: Evidence from resting state fMRI. Parkinsonism Relat. Disord. *94*, 30–36.

36. Kebschull, J.M., Richman, E.B., Ringach, N., Friedmann, D., Albarran, E., Kolluru, S.S., Jones, R.C., Allen, W.E., Wang, Y., Cho, S.W., et al. (2020). Cerebellar nuclei evolved by repeatedly duplicating a conserved cell-type set. Science *370*, eabd5059.

37. Calhoon, G.G., and Tye, K.M. (2015). Resolving the neural circuits of anxiety. Nat. Neurosci. *18*, 1394–1404.

38. Robinson, O.J., Pike, A.C., Cornwell, B., and Grillon, C. (2019). The translational neural circuitry of anxiety. J. Neurol. Neurosurg. Psychiatry *90*, 1353–1360.

39. Cai, H., Haubensak, W., Anthony, T.E., and Anderson, D.J. (2014). Central amygdala PKC-δ(+) neurons mediate the influence of multiple anorexigenic signals. Nat. Neurosci. *17*, 1240–1248.

40. Griessner, J., Pasieka, M., Böhm, V., Grössl, F., Kaczanowska, J., Pliota, P., Kargl, D., Werner, B., Kaouane, N., Strobelt, S., et al. (2021). Central amygdala circuit dynamics underlying the benzodiazepine anxiolytic effect. Mol. Psychiatry *26*, 534–544.

41. Douceau, S., Lemarchand, E., Hommet, Y., Lebouvier, L., Joséphine, C., Bemelmans, A.P., Maubert, E., Agin, V., and Vivien, D. (2022). PKCdelta-positive GABAergic neurons in the central amygdala exhibit tissue-type plasminogen activator: role in the control of anxiety. Mol. Psychiatry *27*, 2197–2205.

42. Zhang, J., Li, B., Yu, L., He, Y.C., Li, H.Z., Zhu, J.N., and Wang, J.J. (2011). A role for orexin in central vestibular motor control. Neuron *69*, 793–804.

43. Ji, M.J., Zhang, X.Y., Chen, Z., Wang, J.J., and Zhu, J.N. (2019). Orexin prevents depressive-like behavior by promoting stress resilience. Mol. Psychiatry *24*, 282–293.

44. Tan, Y., Hang, F., Liu, Z.W., Stoiljkovic, M., Wu, M., Tu, Y., Han, W., Lee, A.M., Kelley, C., Hajós, M., et al. (2020). Impaired hypocretin/orexin system alters responses to salient stimuli in obese male mice. J. Clin. Invest. *130*, 4985–4998.

45. Zhang, X.Y., Yu, L., Zhuang, Q.X., Zhu, J.N., and Wang, J.J. (2013). Central functions of the orexinergic system. Neurosci. Bull. *29*, 355–365.

46. Li, S.B., Damonte, V.M., Chen, C., Wang, G.X., Kebschull, J.M., Yamaguchi, H., Bian, W.J., Purmann, C., Pattni, R., Urban, A.E., et al. (2022). Hyperexcitable arousal circuits drive sleep instability during aging. Science *375*, eabh3021.

47. Sakurai, T. (2014). The role of orexin in motivated behaviours. Nat. Rev. Neurosci. *15*, 719–731.

48. Horvath, T.L., and Gao, X.B. (2005). Input organization and plasticity of hypocretin neurons: possible clues to obesity's association with insomnia. Cell Metab. *1*, 279–286.

49. Schmeichel, B.E., Herman, M.A., Roberto, M., and Koob, G.F. (2017). Hypocretin Neurotransmission Within the Central Amygdala Mediates Escalated Cocaine Self-administration and Stress-Induced Reinstatement in Rats. Biol. Psychiatry *81*, 606–615.

50. Yu, L., Zhang, X.Y., Zhang, J., Zhu, J.N., and Wang, J.J. (2010). Orexins excite neurons of the rat cerebellar nucleus interpositus via orexin 2 receptors in vitro. Cerebellum *9*, 88–95.

51. Islam, M.R., Valaris, S., Young, M.F., Haley, E.B., Luo, R., Bond, S.F., Mazuera, S., Kitchen, R.R., Caldarone, B.J., Bettio, L.E.B., et al. (2021). Exercise hormone irisin is a critical regulator of cognitive function. Nat. Metab. *3*, 1058–1070.

52. Gubert, C., and Hannan, A.J. (2021). Exercise mimetics: harnessing the therapeutic effects of physical activity. Nat. Rev. Drug Discov. *20*, 862–879.

53. Leiter, O., Zhuo, Z., Rust, R., Wasielewska, J.M., Grönnert, L., Kowal, S., Overall, R.W., Adusumilli, V.S., Blackmore, D.G., Southon, A., et al. (2022). Selenium mediates exercise-induced adult neurogenesis and reverses learning deficits induced by hippocampal injury and aging. Cell Metab. *34*, 408–423.e8.

54. Heath, R.G., and Harper, J.W. (1974). Ascending projections of the cerebellar fastigial nucleus to the hippocampus, amygdala, and other temporal lobe sites: evoked potential and histological studies in monkeys and cats. Exp. Neurol. *45*, 268–287.

55. D'Ambra, A.F., Vlasov, K., Jung, S.J., Ganesan, S., Antzoulatos, E.G., and Fioravante, D. (2023). Cerebellar activation bidirectionally regulates nucleus accumbens core and medial shell. Preprint at bioRxiv. https://doi.org/10.7554/eLife.87252.1.

56. Zhang, J., Chen, H., Zhang, L.B., Li, R.R., Wang, B., Zhang, Q.H., Tong, L.X., Zhang, W.W., Yao, Z.X., and Hu, B. (2022). Ventromedial Thalamus-Projecting DCN Neurons Modulate Associative Sensorimotor Responses in Mice. Neurosci. Bull. *38*, 459–473.

57. Ma, K.Y., Cai, X.Y., Wang, X.T., Wang, Z.X., Huang, W.M., Wu, Z.Y., Feng, Z.Y., and Shen, Y. (2021). Three-Dimensional Heterogeneity of Cerebellar Interposed Nucleus-Recipient Zones in the Thalamic Nuclei. Neurosci. Bull. *37*, 1529–1541.

58. Baird, A.D., Wilson, S.J., Bladin, P.F., Saling, M.M., and Reutens, D.C. (2004). The amygdala and sexual drive: Insights from temporal lobe epilepsy surgery. Ann. Neurol. *55*, 87–96.

59. Han, W., Tellez, L.A., Rangel, M.J., Motta, S.C., Zhang, X., Perez, I.O., Canteras, N.S., Shammah-Lagnado, S.J., van den Pol, A.N., and de Araujo, I.E. (2017). Integrated Control of Predatory Hunting by the Central Nucleus of the Amygdala. Cell *168*, 311–324.e18.

Please cite this article in press as: Zhang et al., A role for the cerebellum in motor-triggered alleviation of anxiety, Neuron (2024), https://doi.org/10.1016/j.neuron.2024.01.007

60. Shrestha, P., Shan, Z., Mamcarz, M., Ruiz, K.S.A., Zerihoun, A.T., Juan, C.Y., Herrero-Vidal, P.M., Pelletier, J., Heintz, N., and Klann, E. (2020). Amygdala inhibitory neurons as loci for translation in emotional memories. Nature *586*, 407–411.

61. Feinstein, A., Freeman, J., and Lo, A.C. (2015). Treatment of progressive multiple sclerosis: what works, what does not, and what is needed. Lancet Neurol. *14*, 194–207.

62. Kalia, L.V., and Lang, A.E. (2015). Parkinson's disease. Lancet *386*, 896–912.

63. Schmahmann, J.D., and Caplan, D. (2006). Cognition, emotion and the cerebellum. Brain *129*, 290–292.

64. Stamatakis, E., Ahmadi, M.N., Gill, J.M.R., Thøgersen-Ntoumani, C., Gibala, M.J., Doherty, A., and Hamer, M. (2022). Association of wearable device-measured vigorous intermittent lifestyle physical activity with mortality. Nat. Med. *28*, 2521–2529.

65. Kros, L., Eelkman Rooda, O.H.J., Spanke, J.K., Alva, P., van Dongen, M.N., Karapatis, A., Tolner, E.A., Strydis, C., Davey, N., Winkelman, B.H.J., et al. (2015). Cerebellar output controls generalized spike-and-wave discharge occurrence. Ann. Neurol. *77*, 1027–1049.

66. Tewari, A., Fremont, R., and Khodakhah, K. (2017). It's not just the basal ganglia: Cerebellum as a target for dystonia therapeutics. Mov. Disord. *32*, 1537–1545.

67. Beckinghausen, J., Donofrio, S.G., Lin, T., Miterko, L.N., White, J.J., Lackey, E.P., and Sillitoe, R.V. (2023). Deep Brain Stimulation of the Interposed Cerebellar Nuclei in a Conditional Genetic Mouse Model with Dystonia. In Basic and Translational Applications of the Network Theory for Dystonia (Springer), pp. 93–117.

68. Chang, M., Womer, F.Y., Gong, X., Chen, X., Tang, L., Feng, R., Dong, S., Duan, J., Chen, Y., Zhang, R., et al. (2021). Identifying and validating subtypes within major psychiatric disorders based on frontal-posterior functional imbalance via deep learning. Mol. Psychiatry *26*, 2991–3002.

69. Ding, S.L., Royall, J.J., Sunkin, S.M., Ng, L., Facer, B.A.C., Lesnar, P., Guillozet-Bongaarts, A., McMurray, B., Szafer, A., Dolbeare, T.A., et al. (2016). Comprehensive cellular-resolution atlas of the adult human brain. J. Comp. Neurol. *524*, 3127–3481.

70. Zhuang, Q.X., Li, G.Y., Li, B., Zhang, C.Z., Zhang, X.Y., Xi, K., Li, H.Z., Wang, J.J., and Zhu, J.N. (2018). Regularizing firing patterns of rat subthalamic neurons ameliorates parkinsonian motor deficits. J. Clin. Invest. *128*, 5413–5427.

71. Zhang, X.Y., Peng, S.Y., Shen, L.P., Zhuang, Q.X., Li, B., Xie, S.T., Li, Q.X., Shi, M.R., Ma, T.Y., Zhang, Q., et al. (2020). Targeting presynaptic H3 heteroreceptor in nucleus accumbens to improve anxiety and obsessive-compulsive-like behaviors. Proc. Natl. Acad. Sci. USA *117*, 32155–32164.

72. Zhao, M., Ren, M., Jiang, T., Jia, X., Wang, X., Li, A., Li, X., Luo, Q., and Gong, H. (2022). Whole-Brain Direct Inputs to and Axonal Projections from Excitatory and Inhibitory Neurons in the Mouse Primary Auditory Area. Neurosci. Bull. *38*, 576–590.

73. Kingsbury, L., Huang, S., Wang, J., Gu, K., Golshani, P., Wu, Y.E., and Hong, W. (2019). Correlated Neural Activity and Encoding of Behavior across Brains of Socially Interacting Animals. Cell *178*, 429–446.e16.

74. Yang, Y., Cui, Y., Sang, K., Dong, Y., Ni, Z., Ma, S., and Hu, H. (2018). Ketamine blocks bursting in the lateral habenula to rapidly relieve depression. Nature *554*, 317–322.

75. Wang, Y., Chen, Z.P., Zhuang, Q.X., Zhang, X.Y., Li, H.Z., Wang, J.J., and Zhu, J.N. (2017). Role of Corticotropin-Releasing Factor in Cerebellar Motor Control and Ataxia. Curr. Biol. *27*, 2661–2669.e5.

76. Giardino, W.J., Eban-Rothschild, A., Christoffel, D.J., Li, S.B., Malenka, R.C., and de Lecea, L. (2018). Parallel circuits from the bed nuclei of stria terminalis to the lateral hypothalamus drive opposing emotional states. Nat. Neurosci. *21*, 1084–1095.

77. Peter, S., Ten Brinke, M.M., Stedehouder, J., Reinelt, C.M., Wu, B., Zhou, H., Zhou, K., Boele, H.J., Kushner, S.A., Lee, M.G., et al. (2016). Dysfunctional cerebellar Purkinje cells contribute to autism-like behaviour in Shank2-deficient mice. Nat. Commun. *7*, 12627.

78. Paxinos, G., and Watson, C. (2013). The Rat Brain in Stereotaxic Coordinates, Seventh Edition (Academic Press).

Please cite this article in press as: Zhang et al., A role for the cerebellum in motor-triggered alleviation of anxiety, Neuron (2024), https://doi.org/10.1016/j.neuron.2024.01.007

STAR★METHODS

KEY RESOURCES TABLE

REAGENT or RESOURCE	SOURCE	IDENTIFIER
Antibodies		
rabbit anti-NeuN	Abcam	Cat# ab207281; RRID: AB_2889250
mouse anti-PKCδ	BD Biosciences	Cat# 610398; RRID: AB_397781
rabbit anti-c-Fos	Cell Signaling Technology	Cat# 2250; RRID: AB_2247211
mouse anti-orexin A	R&D Systems	Cat# MAB763; RRID: AB_2117627
mouse anti-GABA	Sigma-Aldrich	Cat# A0310; RRID: AB_476667
mouse anti-glutamate	Millipore	Cat# MAB5304; RRID: AB_94698
rabbit anti-Cre	Abcam	Cat# ab190177; RRID: AB_2860024
rabbit anti-OX2R	Millipore	Cat# AB3094; RRID: AB_91358
goat anti-OX2R	Everest Biotech	Cat# EB10833
goat anti-β-actin	Abcam	Cat# ab8229; RRID: AB_306374
Bacterial and virus strains		
AAV2/9-hSyn-mCherry	OBiO Technology (Shanghai)	AOV063
AAV2/2-Retro-hSyn-eGFP	Shanghai Taitool Bioscience	S0237-2R
AAV2/9-hSyn-DIO-N2cG	Brain Case (Shenzhen)	BC-0304
AAV2/9-hSyn-DIO-TVA-mCherry	Brain Case (Shenzhen)	BC-0061
AAV2/9-hSyn-SV40 NLS-Cre	Brain Case (Shenzhen)	BC-0159
CVS-EnvA-ΔG-eGFP	Brain Case (Shenzhen)	BC-RV-CVS EnvA461
AAV2/9-hSyn-ChrimsonR-tdTomato	BrainVTA (Wuhan)	PT-1432
AAV2/9-hSyn-jGCaMP7f	OBiO Technology (Shanghai)	H11265
AAV2/9-hSyn-hChR2 (H134R)-mCherry	OBiO Technology (Shanghai)	AG26976
AAV2/9-hSyn-oChIEF-tdTomato	Brain Case (Shenzhen)	BC-0451
AAV2/9-CaMKIIα-hChR2 (H134R)-mCherry	OBiO Technology (Shanghai)	AG26975
AAV2/2-Retro-hSyn-Cre-eGFP	Shanghai Taitool Bioscience	S0230-2RP
AAV2/9-hSyn-DIO-hM4D(Gi)-mCherry	Shanghai Taitool Bioscience	S0193-9
AAV2/9-hSyn-DIO-mCherry	Shanghai Taitool Bioscience	S0240-9
AAV2/2-Retro-EF1α-DIO-hM4D(Gi)-eGFP	BrainVTA (Wuhan)	PT-0987
AAV2/2-Retro-EF1α-DIO-eGFP	BrainVTA (Wuhan)	PT-0795
AAV2/9-hEF1a-DIO-eNpHR 3.0-mCherry	Shanghai Taitool Bioscience	S0852-9
AAV2/9-EF1α-DIO-hChR2 (H134R)-eYFP	BrainVTA (Wuhan)	PT-2500
AAV2/2-Retro-Flp-eGFP	BrainVTA (Wuhan)	PT-0803
AAV2/9-EF1α-DIO-eYFP	BrainVTA (Wuhan)	PT-0012
AAV2/9-hSyn-fDIO-hM4D(Gi)-mCherry	BrainVTA (Wuhan)	PT-0170
AAV2/9-hSyn-fDIO-mCherry	BrainVTA (Wuhan)	PT-4158
AAV2/9-CAG-DIO-oChIEF-mCherry	BrainVTA (Wuhan)	PT-3351
AAV2/9-CAG-DIO-mCherry	BrainVTA (Wuhan)	PT-0161
AAV2/9-hEF1a-DIO-eNpHR 3.0-eYFP	Shanghai Taitool Bioscience	S0178-9
AAV2/2-Retro-Cre	Shanghai Taitool Bioscience	S0278-2R
AAV2/1-CaMKIIα-Cre-eGFP	BrainVTA (Wuhan)	PT-0198
AAV2/9-hSyn-DIO-hM3D(Gq)-mCherry	Shanghai Taitool Bioscience	S0192-9

(*Continued on next page*)

Please cite this article in press as: Zhang et al., A role for the cerebellum in motor-triggered alleviation of anxiety, Neuron (2024), https://doi.org/10.1016/j.neuron.2024.01.007

Continued

REAGENT or RESOURCE	SOURCE	IDENTIFIER
AAV-EF1α-DIO-hChR2(H134R)-mCherry	OBiO Technology (Shanghai)	AG20297
LV-CON-eGFP	Shanghai GeneChem	N/A
LV-shOX2R-eGFP	Shanghai GeneChem	N/A
Chemicals, peptides, and recombinant proteins		
NBQX	Tocris Bioscience	Cat# 0373; CAS: 118876-58-7
Tetrodotoxin (TTX)	Alomone Laboratory	Cat# T-500; CAS: 4368-28-9
4-Aminopyridine (4-AP)	Sigma-Aldrich	Cat# 275875; CAS: 504-24-5
Clozapine *N*-oxide dihydrochloride (CNO)	Tocris Bioscience	Cat# 6329; CAS: 2250025-93-3
Ctb 555	Invitrogen	Cat# C34776
Fluoro-Gold™	Abcam	Cat# ab138870
Orexin-A	Tocris Bioscience	Cat# 1455; CAS: 205640-90-0
TCS-OX2-29	Tocris Bioscience	Cat# 3371; CAS: 1610882-30-8
D-AP5	Tocris Bioscience	Cat# 0106; CAS: 79055-68-8
Gabazine	Tocris Bioscience	Cat# 1262; CAS: 104104-50-9
KB-R7943	Tocris Bioscience	Cat# 1244; CAS: 182004-65-5
$BaCl_2$	Sigma-Aldrich	Cat# 342920; CAS: 10361-37-2
Tertiapin-Q	Tocris Bioscience	Cat# 1316; CAS: 910044-56-3
Critical commercial assays		
Orexin A (Human, Rat, Mouse, Porcine, Ovine, Bovine, Monkey) - RIA Kit	Phoenix Pharmaceuticals, inc	Cat# RK-003-30
Experimental models: Organisms/strains		
Rat: Orexin-Cre rats	This paper	N/A
Rat: Sprague-Dawley rats	Vital River (Beijing)	101
Mice: C57BL/6JNifdc Mice	Vital River (Beijing)	219
Software and algorithms		
Clinscan	Bruker Biospin	N/A
MRICron	Neuroimaging Tools and Resources Collaboratory, NITRC)	https://www.nitrc.org/projects/mricron
Advanced Normalization Tools	N/A	https://github.com/ANTsX/ANTs
MAGNETOM Prisma	Siemens Healthineers	N/A
SPM12	The Wellcome Trust Centre for Neuroimaging	https://www.fil.ion.ucl.ac.uk/spm/software/spm12/
DPARSF	N/A	http://rfmri.org/content/dparsf
BioMapping5000	Wuhan OE-Bio Co.Ltd	https://www.oebio-imaging.com/products_details/Biomapping_5000.html
OePreprocessing	Wuhan OE-Bio Co.Ltd	N/A
Amira software (version 2020.1)	Fédération Equestre Internationale	https://www.thermofisher.cn/cn/zh/home/electron-microscopy/products/software-em-3d-vis/amira-software.html
Image Pro Plus	Media Cybernetics	N/A

(*Continued on next page*)

Please cite this article in press as: Zhang et al., A role for the cerebellum in motor-triggered alleviation of anxiety, Neuron (2024), https://doi.org/10.1016/j.neuron.2024.01.007

Continued

REAGENT or RESOURCE	SOURCE	IDENTIFIER
Inscopix Data Acquisition software	Inscopix	version 1.5.3
Inscopix Data Processing Software	Inscopix	version 1.6
Clever TopScan	CleverSys	https://cleversysinc.com/CleverSysInc/automated-behavior-analysis-systems/products/
pClamp 10.0	Molecular Devices	https://www.moleculardevices.com/products/axon-patch-clamp-system
Zeus	Bio-Signal Technologies	N/A
Offline Sorter	Plexon	https://plexon.com/products/offline-sorter/
NeuroExplorer	Nex Technologies	https://www.neuroexplorer.com/
Image J	National Institutes of Health	https://imagej.net/software/imagej/
GraphPad	GraphPad	N/A
Sigmaplot	Systat Software Inc.	N/A

RESOURCE AVAILABILITY

Lead contact

Further information and requests for resources and reagents should be directed to and will be fulfilled by the lead contact, Jing-Ning Zhu (jnzhu@nju.edu.cn).

Materials availability

This study did not generate new unique reagents.

Data and code availability

This study did not generate datasets/code.

EXPERIMENTAL MODEL AND SUBJECT DETAILS

Animals

Orexin-Cre rats, wild-type Sprague-Dawley (SD) rats, and C57BL/6J mice were housed on a 12 h light/dark cycle with ad libitum access to chow food and water. The orexin-Cre rats were generated using CRISPR/Cas9 technology. Briefly, a P2A-Cre cassette was targeted into the coding sequence of exon 2 and right before the stop codon of the orexin gene. The Cas9 mRNA, sgRNA, and targeting vector were co-injected into the cytoplasm of one-cell stage fertilized rat eggs. Injected zygotes were transferred into pseudopregnant female SD rats after 2 h culture in KSOM medium to generate the founder strain, which was maintained on an SD genetic background (Beijing Biocytogen). The F0 chimera rats were crossed with the wild-type rats to gain/achieve the germline transmission F1 rats. The genotyping of the correct P2A-Cre targeted F1 rats was confirmed by PCR, sequencing, and Southern blot. The primers for genotyping are as follows: WT-forward: 5’-GCC ACA CAG GTA CCC TCT CTA CAC -3’ and Mut-reverse: 5’- GTG GGT GGC CTC AAA GAT CCC TTC -3’; Mut-forward: 5’- CTG TGG ATG CCA CCT CTG ATG -3’ and WT-reverse: 5’- CAG GTT TTT CCC GGA GGG CTC AG-3’. EcoRV (3’ Probe-A) and BclI (iCre Probe (5’)) were utilized to cleavage the specific fragments for Southern blot. For further validation of the transgene’s expression, the orexin-Cre rats were crossed with Rosa26-LSL-tdTomato reporter rats (SD-Gt(ROSA)26Sortm1(CAG-LSL-tdTomato)/Bcgen; stock#B-CR-011, Beijing Biocytogen). All experiments, approved by the Animal Ethical and Welfare Committee of Nanjing University, were conducted in accordance with the U.S. National Institutes of Health Guide for the Care and Use of Laboratory Animals.

Human subjects

All participants with bipolar disorder (BD) (n = 52, mean age = 19.85 ± 0.33 years, aged from 18-30) were recruited from the inpatient services at Nanjing Medical University Affiliated Brain Hospital, who were met the following inclusion criteria: (1) met Diagnostic and Statistical Manual of Mental Disorders, Fourth Edition (DSM-IV) diagnostic criteria for BD as determined by trained psychiatrists using the Structured Clinical Interview for DSM-IV Axis I Disorders (SCID), (2) Hamilton Anxiety Rating Scale (HAMA) total score $\geq$ 7. Matched healthy control participants (n = 40, mean age = 21.50 ± 0.24 years, aged from 18-30) met the following inclusion criteria: (1) had no current or lifetime history of an Axis I disorders, (2) had no history of Axis I disorders in first-degree relatives, as determined from a detailed family history, (3) HAMA total score < 7. All participants were excluded if any of the following were present: (1) the existence of substance/alcohol abuse or dependence or concomitant major medical disorders, (2) any magnetic resonance imaging (MRI) contraindications, (3) history of head trauma with loss of consciousness for $\geq$ 5 minutes or any neurological disorder, and

Please cite this article in press as: Zhang et al., A role for the cerebellum in motor-triggered alleviation of anxiety, Neuron (2024), https://doi.org/10.1016/j.neuron.2024.01.007

(4) the presence of a concurrent and major physical illness that could lead to mood disorder symptoms. The HAMA, Hamilton Depression Rating Scale (HAMD) and Young Mania Rating Scale (YMRS) were used to assess symptom severities of anxiety, depression, and mania, respectively. On the same day after these assessments, resting-state functional magnetic resonance imaging data were collected from each participant. The study was approved by the Medical Science Research Ethics Committee of the Nanjing Medical University Affiliated Brain Hospital (approval reference number 2020-KY027-01) and was carried out in accordance with the Helsinki Declaration. All participants provided written informed consent after a complete description of the study.

METHOD DETAILS

Resting-state functional magnetic resonance imaging (fMRI)

Resting-state fMRI in rats

Resting-state fMRI were carried out on a 9.4 T/20 cm horizontal bore animal MRI system (Clinscan, Bruker Biospin). In brief, animals were anesthetized with isoflurane (5% for induction and 2% during experiments) and fixed on a water heating bed. During the functional acquisitions, the breathing rate and body temperature were continuously recorded using a small animal monitor (1030 System, Small Animal Instruments). Resting-state fMRI scans were collected only when physiological parameters remained stable for about 10 min. The fMRI signal was acquired in 5 min and consisted of 52 slices (repetition time (TR) = 2000 ms, echo time (TE) = 6.333 ms, slice thickness = 0.6 mm, field of view (FOV) = 40 × 16 mm^2 and in-plane resolution = 0.4 × 0.4 mm^2). To construct a reference for the brain anatomy, high-resolution (0.281 × 0.281 mm^2, slice thickness = 0.6 mm) structural MRI was acquired using fast spin-echo with TR of 6000 ms, TE of 33 ms, FOV of 36 × 36 mm^2 and average of 3.

The original resting-state data sets were converted into NIFTI format through the dcm2niigui function of the MRICron software. The first 5 TRs of the data were discarded to allow magnetization to reach a steady state. Pre-processing, including slice-timing correction, motion correction, and spatial normalization were performed using the statistical parametric mapping software and advanced normalization tools. Then, blood-oxygen-level-dependent (BOLD) time-courses were extracted from the defined regions of interests (ROIs) for further seed-based connectivity analysis. Pearson's correlation coefficient (*r*-values) between BOLD time-courses from all the ROIs was computed as a measure of functional connectivity. Finally, the statistically significant difference in functional connectivity between the rotarod running and control groups was assessed by a two-sample *t*-test.

Resting-state fMRI in human subjects

Resting-state fMRI was acquired in a 3.0T MRI system (MAGNETOM Prisma, Siemens Healthineers) with a standard 8-channel head coil. The fMRI signal was acquired in 8 min and consisted of 35 slices, the parameters were as follows: TR = 500 ms, TE = 30 ms, slice thickness = 3.5 mm with a 0.5-mm gap, FOV = 224 × 224 mm^2.

As we reported previously,[68] all resting-state fMRI images were preprocessed using SPM12 (https://www.fil.ion.ucl.ac.uk/spm/) and DPARSF (http://rfmri.org/content/dparsf). The first 10 TRs were discarded to allow magnetization to reach a study state. The subsequent preprocessing steps included slice time correction and head motion correction. Next, the functional images were normalized to Montreal Neurological Institute (MNI) space using the EPI template in SPM12, resampled to 3 mm voxels, and then smoothed via a Gaussian kernel with a 6 mm full-width at half-maximum. Linear detrending was performed and several confounding covariates, including the Friston-24 head motion parameters, white matter, cerebrospinal fluid, and global signals, were regressed from the BOLD time series for all voxels. Finally, the resulting data were further temporally band-pass filtered (0.01–0.08 Hz) to reduce the effects of low-frequency drift and high-frequency physiological noises. Then, BOLD time-courses were extracted from the ROIs for further seed-based connectivity analysis. The ROIs were defined as amygdaloid (basolateral nuclear group and central nuclear group) and cerebellar nuclei according to the atlas of the adult human brain.[69] Pearson's correlation coefficient between BOLD time-courses from all the ROIs was computed as a measure of functional connectivity. Finally, correlation analysis was performed between functional connectivity and the HAMA/HAMD/YMRS scale by Pearson's correlation.

Stereotaxic surgery

Male rats weighing 230 to 250 g were anesthetized in an induction chamber (2-4% isoflurane) and placed into a stereotaxic frame (Model 1404, David Kopf Instruments; 68026, Shenzhen Ruiwode Life Technology Co., Ltd.). During the surgery, isoflurane was maintained at 2%, and rats were kept warm on a heating pad. A small hole was drilled in the skull above the site of interest (Bregma coordinates in mm: centrolateral amygdala (CeL), -2.16 AP, ±4.4 ML, 8.1 DV; centromedial amygdala (CeM), -2.16 AP, ±3.9 ML, 8.1 DV; dentate nuclei (DN), -11.28 AP, ±3.6 ML, 6.2 DV; fastigial nucleus (FN), -11.40 AP, ±1.2 ML, 6.0 DV; interposed nucleus (IN), -11.52 AP, ±2.5 ML, 6.0 DV; perifornical area (PFA), -2.76 AP, ±1.4 ML, 8.4 DV) to facilitate further microinjection or intracranial implantation. For rats receiving a virus or drug microinjection, a blunt needle (86200, Hamilton) syringe was used to deliver the vector or drug at a rate of 100 nL/min. For rats receiving intracranial implants, including GRIN lens, optogenetic optic fibers, multielectrode array, and cannulas, the implant was slowly lowered to the target site, and secured to the skull using bone screws and C&B-metabond quick adhesive luting cement (Parkell Prod) or dental cement. The effective extent of the drug diffusion in the present study was restricted in the target nucleus according to the estimate by an extracellular electrophysiological recording of units 0.5-2.0 mm away from the injection site as our previous reports.[42,70] Data from rats in which the injection or implantation sites were histologically identified to be deviated from the target brain regions were excluded from further analysis. The viruses and drugs injected for each experiment are listed in key resources table.

Please cite this article in press as: Zhang et al., A role for the cerebellum in motor-triggered alleviation of anxiety, Neuron (2024), https://doi.org/10.1016/j.neuron.2024.01.007

Anatomical tracing

The experimental procedures for anterograde and retrograde tracing followed our previous reports.[43,70,71] For anterograde and retrograde tracing of the cerebello-amygdalar circuit in rats, virus AAV2/9-hSyn-mCherry and AAV2/2-Retro-hSyn-eGFP were stereotaxically microinjected into the cerebellar nuclei, including the DN, IN and FN, and the CeL, respectively. For labeling the hypothalamic orexinergic neurons that project to the cerebellum and/or amygdala, retrograde tracers Fluoro-Gold and Ctb 555 were microinjected into the DN and CeL, respectively. Three weeks later, rats were euthanized and 30-μm-thick coronal brain slices were prepared. Images were taken at 300 μm intervals from central amygdala (-1.56 mm to -2.76 mm relative to Bregma), at 120 μm intervals from CN (-10.92 mm to -11.76 mm relative to Bregma), and at 150 μm intervals from PFA (-2.28 mm to -3.48 mm relative to Bregma) using a confocal microscope (STP 8000, Leica or LSM 880, Zeiss).

For trans-monosynaptic retrograde rabies tracing in mice,[72] 60 nL of AAV helper virus was injected into the CeL (-1.22 AP, ±2.45 ML,4.63 DV) with a microsyringe pump (QSI 53311, Stoeling). The helper virus included two viruses (1: 2), AAV2/9-hSyn-SV40 NLS-Cre: RMT-mCherry-1/5-N2c (generated by co-package of AAV2/9-DIO-TVA-mCherry and AAV2/9-DIO-N2cG at a ratio of 1:5). Two weeks later, 150 nL of RV (CVS-EnVA-ΔG-EGFP) was injected into the same area and allowed to express for another seven days.

For trans-monosynaptic anterograde tracing in rats, AAV2/1-CaMKII-Cre-eGFP virus was injected into the DN (-11.28 AP, ±3.6 ML, 6.2 DV), and AAV2/9-hSyn-DIO-mcherry virus was injected into the CeL (-2.16 AP, ±4.4 ML, 8.1 DV). Three weeks later, rats were perfused and brains were removed for fixation.

For quantitative analysis of the anterogradely labeled projections, the density of cerebellar nucleofugal fibers in the amygdala was assessed by the surface area (μm^2) occupied by mCherry-positive signals per μm^2 of the basolateral amygdala, CeL, and CeM. For quantitative analysis of the retrogradely labeled neurons, the number of eGFP-positive cells in the FN, IN, and DN, as well as Fluoro-Gold and Ctb 555 positive neurons in the PFA were counted.

Fluorescence Micro-optical Sectioning Tomography (fMOST)

Tissue processing

After anesthetized, mice were transcardially perfused with PBS, followed by 4% cold paraformaldehyde (PFA). The brains were post-fixed in 4% PFA at 4°C for over 24h, and then rinsed with PBS at 4°C for 24 h, and subsequently dehydrated with a graded ethanol solution of 50%, 75%, and 95% (each gradient for 2h), and then soaked in 100% ethanol overnight at 4°C. Next, brains were immersed in a graded LR White resin solution (containing 0.3% SBB) of 50%, 75% (each gradient for 2h), then soaked in 100% LR White resin solution for 2 days, and finally cured for 12 h in an oven at 48°C.

fMOST imaging

The brains were installed in the fMOST system (BioMapping5000, Wuhan OE-Bio Co., Ltd), which uses lasers (473 nm and 561 nm, Cobolt) as excitation light source, 40× water immersion eyepiece (0.8 NA, LUMPLFLN, Olympus) and TDI-CCD (4K, DALSA) for signal detection. Brains were cut into ultrathin slices (thickness = 2 μm) continuously, and at the same time, the slices were imaged in turn. A total of about 6000 coronal sections constituted the whole brain data set.

Image registration

The imaging data was registered to Allen Common Coordinate Framework (CCFv3) and corrected with rigid registration. More specifically, overall the brain used greyscale-based 3D affine registration, meanwhile regions of interest (ROIs) used dense landmark-based 2D registration. Subsequently, the neurons in ROIs were transformed into Allen Brain Atlas space. There were always two experienced analysts who checked the image registration results by manual confirmation independently.

Single-cell reconstruction

In order to improve the signal-to-noise ratio of imaging data, image preprocessing procedures were performed by OePreprocessing (Wuhan OE-Bio Co., Ltd.), including image stitching, brightness adjustment, and noise filtering. Amira software (version 2020.1, Fédération Equestre Internationale) was applied for tracing the neurite skeletons between the image stacks by the filament editor module. Throughout the process, there always were two experienced annotators who traced each neuron in the cerebellar nuclei independently and then compared their reconstructions to produce a final consensus.

Immunohistochemistry

Rats were anesthetized with sodium pentobarbital (40 mg/kg) and perfused transcardially with 200 mL of saline, followed by 250-300 mL of 4% sodium phosphate-buffered paraformaldehyde. Brains were post-fixed in the same fixative for 12 h at 4 °C, then cryoprotected with 20% and 30% sucrose for 48 h respectively. Frozen coronal sections (30 μm thick) containing CN, CeL, or PFA were obtained by using a freezing microtome (CM3050S, Leica) and mounted on gelatin-coated slides. The slices were rinsed with PBS containing 0.1% Triton X-100 (PBST) and then incubated in 10% normal bovine serum in PBST for 30 min. Sections were incubated overnight at 4°C with primary antibodies. After a complete wash in PBS, the sections were incubated in the related conjugated secondary antibodies with a fluorescent label for 2-3 h at room temperature in the dark. The slides were washed and mounted in Fluoromount-G mounting medium (F4680, Southern Biotech). Incubations replacing the primary antiserum with control immunoglobulins and/or omitting the primary antiserum were used as negative controls. All micrographs were taken with Leica STP 8000 or Zeiss LSM 880 confocal microscope, equipped with Plan-Apochromat × 60/1.42 NA oil, × 40/0.9 NA dry, × 20/0.75 NA dry, and × 10/0.4 NA dry objective lenses. Digital images from the microscope were recorded with Leica Application Suite (v2.5.0 R1) and image processing was done with Image Pro Plus (6.0, Media Cybernetics). Quantification of c-Fos immunoreactive neurons in the amygdala

Please cite this article in press as: Zhang et al., A role for the cerebellum in motor-triggered alleviation of anxiety, Neuron (2024), https://doi.org/10.1016/j.neuron.2024.01.007

and PFA was blindly counted by two independent investigators. Experimental conditions were repeated at least 3 times to account for technical and biological variation. The primary antibodies for each experiment are listed in key resources table.

Miniscope Ca^{2+} imaging in freely moving rats

The activity of GCaMP7f-labeled CeL neurons during rotarod running (10 rpm), optogenetic activation of the DN neurons (30 Hz, 5 ms-pulse width), and rotarod running (10 rpm) with optogenetic silencing of the DN-CeL projections (constant light, 8 s on/2 s off) was imaged using the miniature microscope (nVista 3.0, Inscopix) with an integrated blue LED (475 nm, average power 1 mW/mm^2).[73] To avoid optogenetic activation/inhibition of the DN terminals within CeL by the blue LED integrated with a miniature microscope, yellow light-activated ChrimsonR/eNpHR was used for optogenetic activation/inhibition of the DN/DN^{CeL} neurons (Figures 2C–2G and S3). Before the experiments, a baseplate (BLP-2, Inscopix) was assembled to help mount the miniscope onto the skull and fix the working distance between the microscope objective and GRIN lens at the most optimal focal length. Ca^{2+} imaging was acquired using Inscopix Data Acquisition software (v1.5.3, Inscopix) at a frame rate of 20 Hz with a light-emitting diode power of 50% (1.0 mW at the objective, 475 nm), gain of 4, a field of view of 1280 × 800 pixels and microscope focus of 320 μm. Time stamps of imaging frames and behavioral coordinates were collected for alignment using the synchronized video. Moreover, the nVista system was synchronized with optogenetic device via the trigger port.

Post-acquisition processing of Ca^{2+} imaging videos was performed using the Inscopix Data Processing Software (IDPS, version 1.6, Inscopix). Videos were downsampled both spatially and temporally by a factor of 2. Motion correction was performed by shifting each frame to a single reference frame so that high contrast features within each frame were aligned to the corresponding features in the reference frame. Normalized fluorescence changes were then visualized in a $\Delta F/F0$ video, in which a minimum z-projection image of the entire movie (F0) was subtracted from each frame (F), and the resultant F–F0 movie was normalized to F0. PCA-ICA was used to identify cells in the $\Delta F/F0$ video, followed by human visual verification against the $\Delta F/F0$ video, in which candidate cells that did not show appropriate cell morphology and fluorescence intensity changes were removed manually from further analysis. Ca^{2+} transient events were detected using a Ca^{2+} event detection algorithm in IDPS (parameters, event smallest decay time = 0.20 s, event threshold factor = 5 median absolute deviation) by finding large peaks of fluorescence changes with fast rise times and exponential decay.

Optogenetic and chemogenetic manipulation

As we reported previously,[71] the single end of 2 × 1 fiber splitter (Newdoon) was connected to a rotating commutator (Doric), which was then attached via a fiber to a laser (Newdoon). Light output was measured with an optical power meter and adjusted to 7 mW of 590 nm or 473 nm light. To mimic the activation of DN^{CeL} neurons during constant rotarod running (10 rpm), yellow or blue light was applied at 5-ms pulse width with a frequency of 30 Hz (Figures 2C–2G, 3K, 3L, 7C–7F, and S5G–S5J). To inhibit DN^{CeL} neurons during constant rotarod running (10 rpm), yellow light was applied at 5-ms pulse width (constant light, 8 s on/2 s off) (Figures 6D–6F and S3). oChIEF which allows for reliable responses to sustained high-frequency optostimulation was applied[74] for opto-activation of DN^{CeL} neurons to reach their firing rate during accelerating rotarod running (acceleration of 0.2 rpm/s), blue light was employed at a 5-ms pulse width with a frequency of 60 Hz (Figures 7C–7F). For optostimulation of PFA-DN orexinergic afferent terminals, blue light with 10-ms pulse width and a frequency of 20 Hz was delivered (Figures 5C, 5D, 6G, and 6H).

For chemogenetic activation or inhibition of CN-CeL or PFA-DN circuit, clozapine N-oxide dihydrochloride (CNO; 2 mg/kg, 6329, Tocris Bioscience) was administered by intraperitoneal/intra-CeL injection 30 min before rotarod running or behavioral tests. Moreover, to rule out the possibility of CNO itself influencing the experimental results, CNO administration in hM3Dq/hM4Di negative rats was set as control groups.

Behavioral tests

Animals were randomly assigned to different treatment groups. Each group of animals was subjected to a separate behavioral test and received no additional human handling. All behavioral experiments and data analysis were performed blind to the conditions of the experiments. All tests started at the same time (9:00 a.m.) each day.

Rotarod running

To assess the effect of general and challenging movement on anxiety, rotarod running at a constant (10 rpm) or an accelerating (from 5 to 40 rpm, with an acceleration of 0.12, 0.2, or 0.4 rpm/s) speed was applied respectively by using a commercially available rotarod (Ugo Basile). Animals were subjected to 6 trials of constant/accelerating rotarod running per day, with time limits of 240 s/trial and a 240 s resting interval to avoid stress and fatigue. For control group, each rat was placed in an individual compartment of the rotarod, which kept stationary. According to our previous reports,[42,75] rats that perform constant and accelerating rotarod running can achieve their best performance before or on the third day. Therefore, the elevated plus maze and light/dark box tests were examined 30 min after constant or accelerating rotarod running on the fourth day to evaluate the effect of general and challenging movements on anxiety-like behaviors.

Elevated plus maze

The elevated plus maze is a widely used test for assessing anxiety-like behavior.[76] As we reported previously,[43,71] the apparatus consists of two open arms (50 cm × 12 cm) and two closed arms (50 cm × 12 cm with walls 40 cm in height) that are intersected at a central square (15 cm × 15 cm), with a height of 50 cm from the ground. Rats were placed in the center with their heads facing an open

Please cite this article in press as: Zhang et al., A role for the cerebellum in motor-triggered alleviation of anxiety, Neuron (2024), https://doi.org/10.1016/j.neuron.2024.01.007

arm, and their behaviors were recorded in a 5-min test period. The time spent on the open arms and the percentage of open arms entries were recorded and analyzed as anxiety measures using Clever TopScan (Clever Sys).

Light/dark box test

The light/dark box test apparatus consists of a light box (30 cm × 30 cm × 30 cm), a dark box (30 cm × 30 cm × 30 cm), and a passage (8 cm × 8 cm) between the light box and the dark box. According to our previous studies,[43,71] rats were placed into the middle of the light box facing the black box. The total time spent in the light box in a 10-min test period and the total distance run in the apparatus were measured using Clever TopScan (Clever Sys).

Chronic unpredictable mild stress (CUMS)

The CUMS procedure was performed to test the improvement of movement on stress-induced anxiety. In brief, rats were exposed to 14 days of chronic unpredictable mild stressors, including water deprivation for 12 h, food deprivation for 12 h, reversed light/dark cycle for 24 h, physical restraint for 2 h, soiled bedding (200 mL water in 100 g sawdust bedding) for 24 h, a 45° cage tilt for 12 h, and a crowded cage for 12 h.

Patch-clamp recordings in brain slices

Brain slices containing the CeL or DN were prepared and whole-cell patch-clamp recordings were performed as previously described[43,71,75,77] with borosilicate glass pipettes (3-5 MΩ), which were filled with (in mM): 140 K-methylsulfate, 7 KCl, 2 $MgCl_2$, 10 HEPES, 0.1 EGTA, 4 Na_2-ATP, 0.4 GTP-Tris, and 4% biocytin (Sigma, B4261), pH 7.25. Briefly, patch-clamp recordings were acquired with an Axopatch-200B amplifier (Axon Instruments) and the signals were fed into a computer through a Digidata-1550 interface (Axon Instruments) for data capture and analysis (pClamp 10.0, Axon Instrument). Recordings of whole-cell currents were low-pass filtered at 2 kHz and digitized at 10 kHz and recordings of membrane potentials were low-pass filtered at 5 kHz and digitized at 20 kHz. Neurons were held at a membrane potential of -60 mV and characterized by injection of rectangular voltage pulse (5 mV, 50 ms) to monitor the whole-cell membrane capacitance, series resistance, and membrane resistance. Neurons were excluded from the study if the series resistance was not stable or exceeded 25 MΩ.

We filled all recorded neurons with biocytin and then immunostained them with glutamate, GABA (Figures 6A and 6B), or PKCδ (Figure 3J) after recordings. The recorded glutamatergic DN projection neurons co-labeled with biocytin and glutamate in this study had large size (somata diameters > 20 μm), characteristically exhibited complex waveform of afterpotentials, and showed a shift from spontaneous regular tonic firing pattern to bursts of high-rate firing that were separated from each other by intervals of quiescence in response to continuous intracellular injection of hyperpolarizing current (Figure S6B). On the contrary, the recorded GABAergic CN interneurons had small size (somata diameters < 10 μm), and characteristically exhibited afterpotential only exhibited a slow afterhyperpolarization and a shut off of firing in response to constant hyperpolarization (Figure S6D).

We assessed the responses of the glutamatergic and GABAergic CN neurons to orexin-A, by both current-clamp and voltage-clamp recordings. After each brief bath application (1 min) of orexin-A (100 nM, 1455, Tocris Bioscience), cells were given at least 20 min for recovery and prevention of desensitization. To further explore the underlying ionic mechanisms, selective Na^+-Ca^{2+} exchanger blocker KB-R7943 (50 μM, 1244, Tocris Bioscience), broad-spectrum potassium channel blocker $BaCl_2$ (1 mM, 342920, Sigma), and selective inward rectifier potassium channel blocker Tertiapin-Q (0.1 μM, 1316, Tocris Bioscience) were used (Figures 6C, S6G, S6I, and S6J). The ion exchanger/channel blocker was given for at least 15 min before we observed its effect.

For optogenetic stimulation, 470-nm light pulses were applied with a system (pE-300white, CoolLED) attached to the upright microscope (BX51WI, Olympus; MP-1000, Scientifica Ltd.). The optostimulation protocol was 5 ms pulses, 1 pulse in 30 s for recording of light-evoked EPSCs at DN-CeL synapse. Blue light was delivered at 100 Hz for 1 s, and repeated 3 times 20 s apart for high-frequency stimulation of the DN glutamatergic terminals in CeL and LTP induction. Maximal light output at 470 nm was measured at 2 mW by an optical power meter (Thorlabs). To confirm the monosynaptic glutamatergic input from DN neurons to the CeL, the selective AMPA receptor antagonist NBQX (20 μM, 0373, Tocris Bioscience), the selective voltage-gated sodium channel blocker tetrodotoxin (TTX; 0.3 μM, T-500, Alomone Laboratory), and relatively selective A-type K^+ channel blocker 4-aminopyridine (4-AP; 500 μM, A1910, Sigma) were used.

Multielectrode array recordings *in vivo*

To record the activities of DN^{CeL} neurons during rotarod running or optogenetic/pharmacological manipulation, a multi-channel microelectrode array (MWA-16, Bio-Signal Technologies) composed of 16 nickel-chromium wires (35 μm in diameter, 4 × 4 array, measuring range of about 0.5 mm × 0.5 mm) for recording, integrated with an optical fiber (diameter of 200 μm, length of 7 mm, Newdoon) or a guide cannulae (external catheter, outer diameter of 410 μm, inner diameter of 250 μm; inner catheter, outer diameter of 210 μm, inner diameter of 110 μm, length of 7 mm, RIWARD) in the center for optogenetic or pharmacological manipulation, were produced as we reported previously.[70] Broadband (0.3-7.5 kHz) neural signals were simultaneously recorded (16 bits@30 kHz) from implanted 16-arrays using a multichannel data acquisition system (Zeus, Bio-Signal Technologies). Spikes were extracted with high-pass (300 Hz) filters. Real-time spike sorting was performed using principal component analysis. Offline Sorter (Plexon) was used for spike sorting refinement before analyzing data in NeuroExplorer (Nex Technologies).

Please cite this article in press as: Zhang et al., A role for the cerebellum in motor-triggered alleviation of anxiety, Neuron (2024), https://doi.org/10.1016/j.neuron.2024.01.007

Enzyme-linked immunosorbent assay (ELISA)

After a constant or accelerating rotarod running, rats were anesthetized with isoflurane then decapitated to obtain the whole brain. The tissue of DN was collected from coronal brain slices of the rats according to the rat brain atlas of Paxinos and Watson[78] in a freezing microtome (CM3050S, Leica). The brain tissue samples were weighed and immersed in 0.5 M acetic acid and then boiled for 10 min. The samples were centrifuged for 30 s at 5000 rpm and the supernatants were freeze-dried, and the dried samples were subsequently stored at -80°C. Orexin-A kit (FEK-003-30, Phoenix Pharmaceuticals) was used for the ELISA testing. Upon completion of the assays, the fluorescence intensities of the 96 well microplates were read by microplate reader (Tecan). After averaging the results of duplicate wells, orexin value was calculated as pg/mg wet tissue.

Western blot

For western blot analysis, tissue lysate from dissected rat DN was used. Tissue was homogenized in cold RIPA lysis buffer (P0013B, Beyotime) containing protease and phosphatase inhibitors, and lysed for 30 min. Lysates were cleared by centrifugation at 12000 rpm for 20 min. Protein concentration was measured by using A660 kit (Pierce Rockford, IL), and equal amount of protein (30 μg) for each sample was separated by SDS-PAGE gel (10%) and then transferred to polyvinylidene fluoride (PVDF) membrane by electroblotting. The membrane was blocked by non-fat milk (5%) in Tris-buffered saline containing 0.1% Tween 20 and incubated overnight at 4°C with primary antibody: goat anti-orexin receptor 2 (1:1000, EB10833, Everest), goat anti-β-actin (1:500, ab8229, Abcam). The membrane was washed 3 times with TBST (TBS containing 0.1% Tween 20) after 1-h incubation at room temperature with secondary antibodies including horseradish peroxidase (HRP)-conjugated goat anti-rabbit IgG (1:10000, 31460, Thermo Scientific), and HRP-conjugated rabbit anti-goat IgG (1:10000, 81-1620, Thermo Scientific) followed by visualization with chemiluminescence and exposed to Kodak medical X-ray film (Denville Scientific Inc). Protein band intensity was quantified using Image J software (National Institutes of Health), and the relative expression level of respective proteins was calculated by normalization to the Actin protein.

QUANTIFICATION AND STATISTICAL ANALYSIS

All data were analyzed with Graphpad 7.0 and Sigmaplot, and presented as mean ± SEM. The Student's t test and one-way/two-way analysis of variance (ANOVA) were employed for statistical analysis, and Tukey's/Dunnett's/Newman-Keuls post hoc testing was used to further determine the differences between groups. P values of < 0.05 were considered to be significant. The detailed statistical results for each experiment are summarized in Table S1.

Neuron, Volume *112*

Supplemental information

A role for the cerebellum in motor-triggered alleviation of anxiety

Xiao-Yang Zhang, Wen-Xia Wu, Li-Ping Shen, Miao-Jin Ji, Peng-Fei Zhao, Lei Yu, Jun Yin, Shu-Tao Xie, Yun-Yong Xie, Yang-Xun Zhang, Hong-Zhao Li, Qi-Peng Zhang, Chao Yan, Fei Wang, Chris I. De Zeeuw, Jian-Jun Wang, and Jing-Ning Zhu

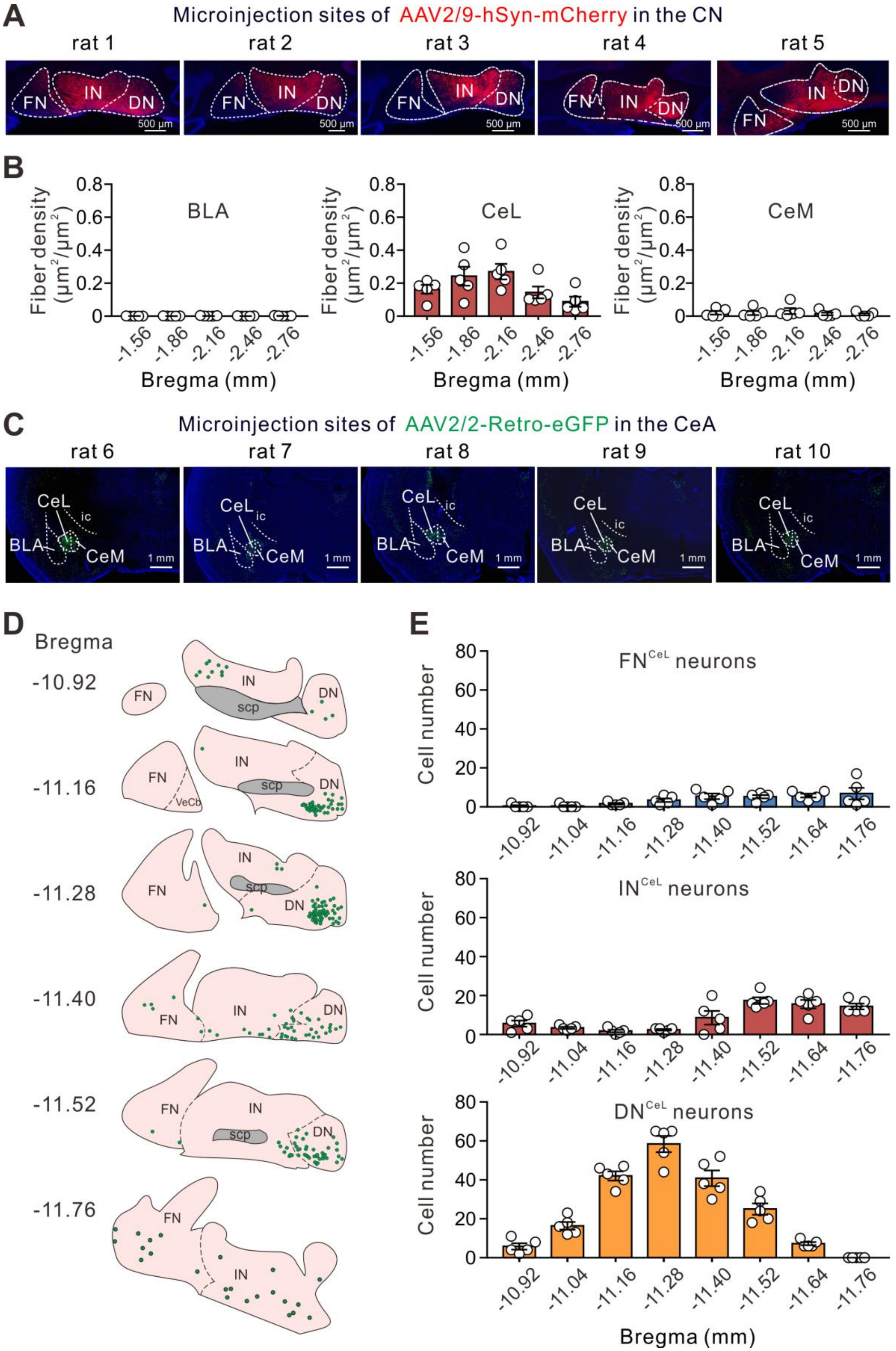
A
Microinjection sites of AAV2/9-hSyn-mCherry in the CN
rat 1
rat 2
rat 3
rat 4
rat 5
FN
IN
DN
500 μm
B
Fiber density (μm²/μm²)
0.8
0.6
0.4
0.2
0
BLA
CeL
CeM
-1.56
-1.86
-2.16
-2.46
-2.76
Bregma (mm)
C
Microinjection sites of AAV2/2-Retro-eGFP in the CeA
rat 6
rat 7
rat 8
rat 9
rat 10
CeL
ic
BLA
CeM
1 mm
D
Bregma
-10.92
-11.16
-11.28
-11.40
-11.52
-11.76
FN
IN
DN
scp
VeCb
E
Cell number
80
60
40
20
0
FN^CeL neurons
IN^CeL neurons
DN^CeL neurons
-10.92
-11.04
-11.16
-11.28
-11.40
-11.52
-11.64
-11.76
Bregma (mm)

Figure S1. Anterograde and retrograde tracing of the cerebello-amygdalar circuit in rats, related to Figure 1

(A) Coronal sections showing microinjection sites of anterograde viral tracer AAV-hSyn-mCherry in the cerebellar nuclei (FN, IN and DN) for all 5 rats.

(B) Statistics of the density of mCherry-positive fibers along the anterior-posterior axis of the basolateral (BLA), centrolateral (CeL) and centromedial (CeM) amygdala (n = 5 rats).

(C) Images of microinjection sites of the retrograde viral tracer AAV-Retro-eGFP in CeL and CeM.

(D) Reconstruction of the distribution pattern of the cerebello-amygdalar projection neurons in CN.

(E) Statistics of the FN^{CeL}, IN^{CeL} and DN^{CeL} neurons along the anterior-posterior axis of the cerebellum; it should be noted that the numbers reflect the total number of labeled cells observed in the five rats involved, highlighting the relative sparseness of the projection (n = 5 rats).

BLA, Basolateral amygdala; CeL, centrolateral amygdala; CeM, centromedial amygdala; DN, dentate nucleus, FN, fastigial nucleus; ic, internal capsule; IN, interposed nucleus; scp, superior cerebellar peduncle. Data are mean ± SEM. For statistics, see Table S1.

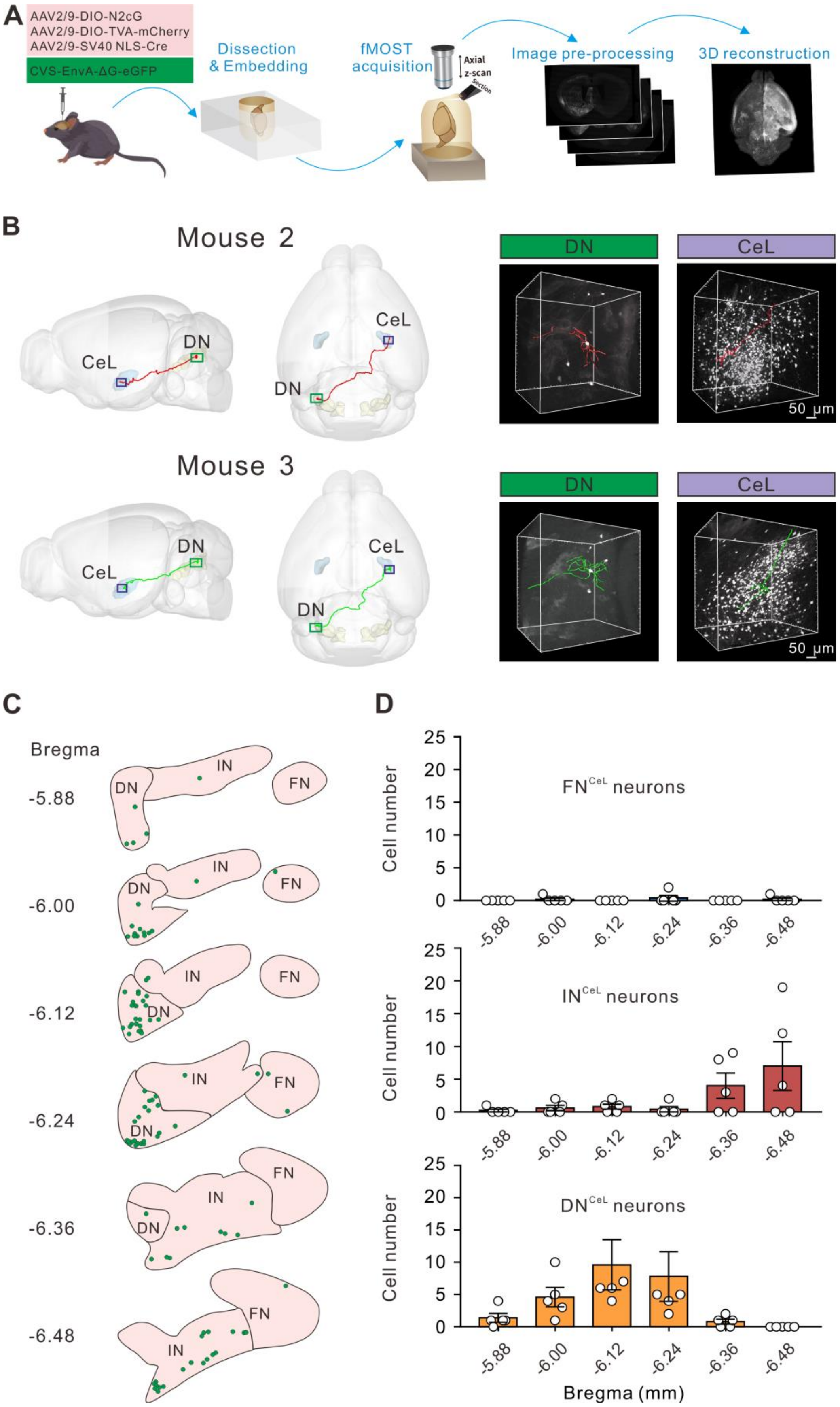
A
AAV2/9-DIO-N2cG
AAV2/9-DIO-TVA-mCherry
AAV2/9-SV40 NLS-Cre
CVS-EnvA-ΔG-eGFP
Dissection
& Embedding
fMOST
acquisition
Axial
z-scan
Section
Image pre-processing
3D reconstruction
B
Mouse 2
CeL
DN
CeL
DN
DN
CeL
50 μm
Mouse 3
DN
CeL
CeL
DN
DN
CeL
50 μm
C
Bregma
-5.88
-6.00
-6.12
-6.24
-6.36
-6.48
DN
IN
FN
D
Cell number
FN^CeL neurons
IN^CeL neurons
DN^CeL neurons
25
20
15
10
5
0
-5.88
-6.00
-6.12
-6.24
-6.36
-6.48
Bregma (mm)

Figure S2. Trans-monosynaptic retrograde rabies tracing of the cerebello-amygdalar circuit in mice, related to Figure 1

(A) Scheme of RV-mediated monosynaptic retrograde tracing and main steps of data acquisition and analysis for retrograde tracing using fMOST.

(B) Sagittal and horizontal views demonstrating the axonal morphologies of the two DN neurons projecting to CeL shown in red (upper left) and green (bottom left). Raw data (upper and bottom right) with a volume of $0.5 \times 0.5 \times 0.5$ mm^3 containing two DN neurons, the passing fibers, and their targeting CeL neurons from the corresponding 2 mouse brains show in the upper and bottom left.

(C) Reconstruction of the distribution pattern of the cerebello-amygdalar projection neurons in CN.

(D) Statistics of the FN^{CeL}, IN^{CeL} and DN^{CeL} neurons along the anterior-posterior axis of the cerebellum. Note that the numbers reflect the total number of labeled cells observed in the five mice involved (three mice for fMOST and two for confocal microscopy imaging), highlighting the relative sparseness of the projection (n = 5 mice).

CeL, centrolateral amygdala; DN, dentate nucleus, FN, fastigial nucleus; IN, interposed nucleus. Data are mean ± SEM. For statistics, see Table S1.

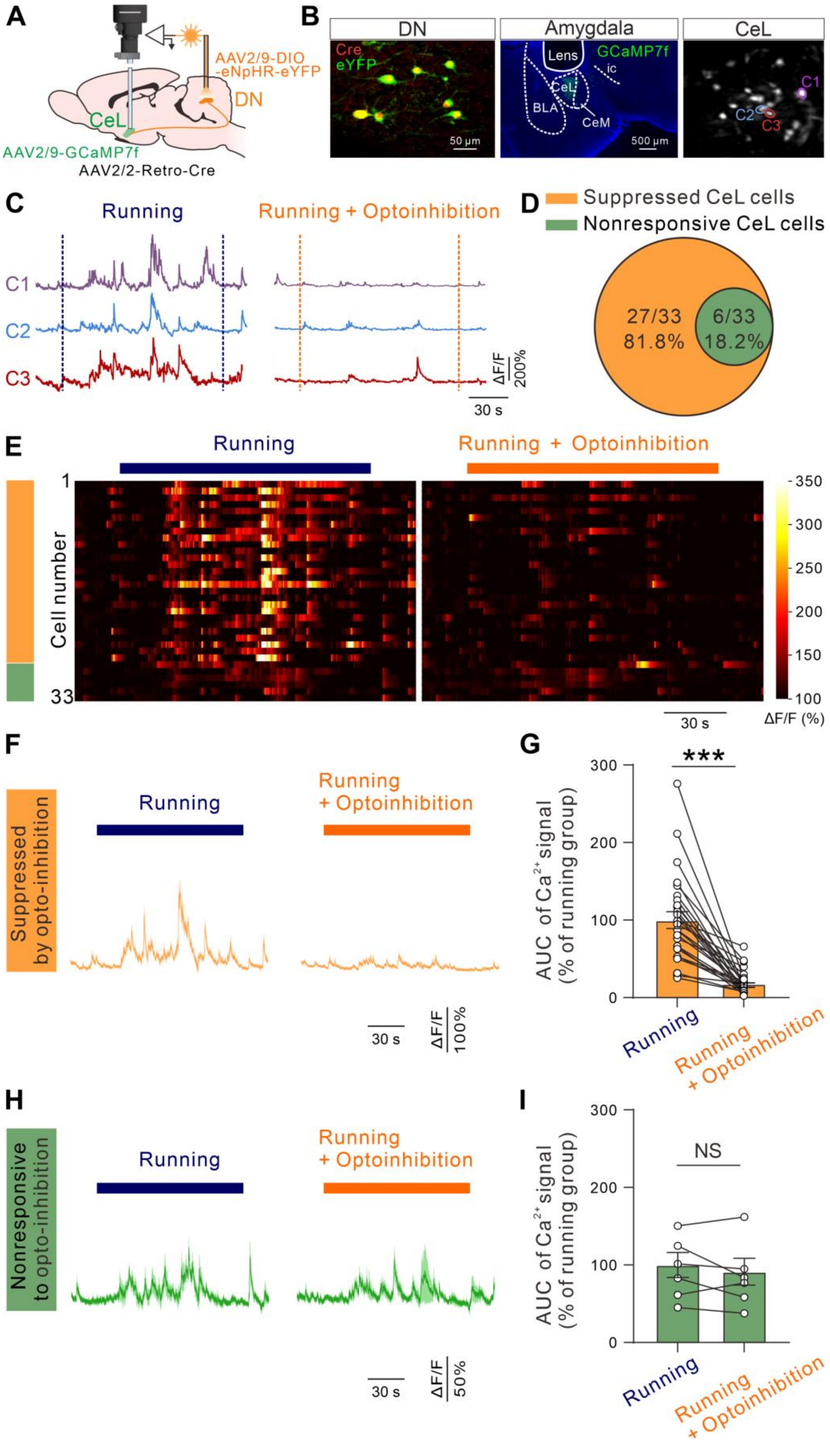
A
AAV2/9-DIO
-eNpHR-eYFP
DN
CeL
AAV2/9-GCaMP7f
AAV2/2-Retro-Cre
B
DN
Cre
eYFP
50 µm
Amygdala
Lens
GCaMP7f
ic
CeL
BLA
CeM
500 µm
CeL
C1
C2
C3
C
Running
Running + Optoinhibition
C1
C2
C3
ΔF/F
200%
30 s
D
Suppressed CeL cells
Nonresponsive CeL cells
27/33
81.8%
6/33
18.2%
E
Running
Running + Optoinhibition
1
Cell number
33
30 s
350
300
250
200
150
100
ΔF/F (%)
F
Suppressed by opto-inhibition
Running
Running + Optoinhibition
30 s
ΔF/F
100%
G
***
300
200
100
0
AUC of Ca2+ signal (% of running group)
Running
Running + Optoinhibition
H
Nonresponsive to opto-inhibition
Running
Running + Optoinhibition
30 s
ΔF/F
50%
I
300
200
100
0
NS
AUC of Ca2+ signal (% of running group)
Running
Running + Optoinhibition

Figure S3. Opto-inhibition of DN neurons projecting to CeL suppresses the responses of CeL neurons to rotarod running, related to Figure 2

(A) Schematic of GCaMP7f and Cre-dependent eNpHR virus microinjection in the centrolateral amygdala (CeL) and cerebellar dentate nucleus (DN), respectively, and microendoscopic calcium imaging in the CeL using a miniscope combined with a GRIN lens.

(B) Images of Cre-dependent eNpHR expression in DN neurons projecting to CeL (left), GCaMP7f expression (green) and GRIN lens location in CeL (middle), and microendoscopic calcium imaging in CeL (right).

(C) Calcium traces from 3 recorded CeL neurons showing that the calcium signals activated by rotarod running are largely suppressed by opto-inhibition of DN neurons projecting to CeL (DN^{CeL}).

(D) Proportions of rotarod running-activated CeL neurons suppressed by/nonresponsive to opto-inhibition of DN^{CeL} neurons (n = 33 cells from 4 rats).

(E) Heat maps of normalized $\Delta F/F$ traces illustrating the response kinetics of rotarod running-activated CeL neurons suppressed (indicated by orange) by/nonresponsive (indicated by green) to opto-inhibition of DN^{CeL} neurons (n = 33 cells from 4 rats).

(F) Averaged calcium traces of the recorded running-activated CeL neurons suppressed by opto-inhibition of DN^{CeL} neurons (n = 27 cells from 4 rats).

(G) The area under the curve (AUC) of calcium traces from the recorded running-activated CeL neurons suppressed by opto-inhibition of DN^{CeL} neurons (n = 27 cells from 4 rats).

(H) Averaged calcium traces of the recorded running-activated CeL neurons nonresponsive to opto-inhibition of DN^{CeL} neurons (n = 6 cells from 4 rats).

(I) The area under the curve (AUC) of calcium traces from the recorded running-activated CeL neurons nonresponsive to opto-inhibition of DN^{CeL} neurons (n = 6 cells from 4 rats).

BLA, basolateral amygdala; CeM, centromedial amygdala; ic, internal capsule. Data are mean ± SEM. Paired t test for (G and I). ***$P < 0.001$; NS, not significant. For statistics, see Table S1.

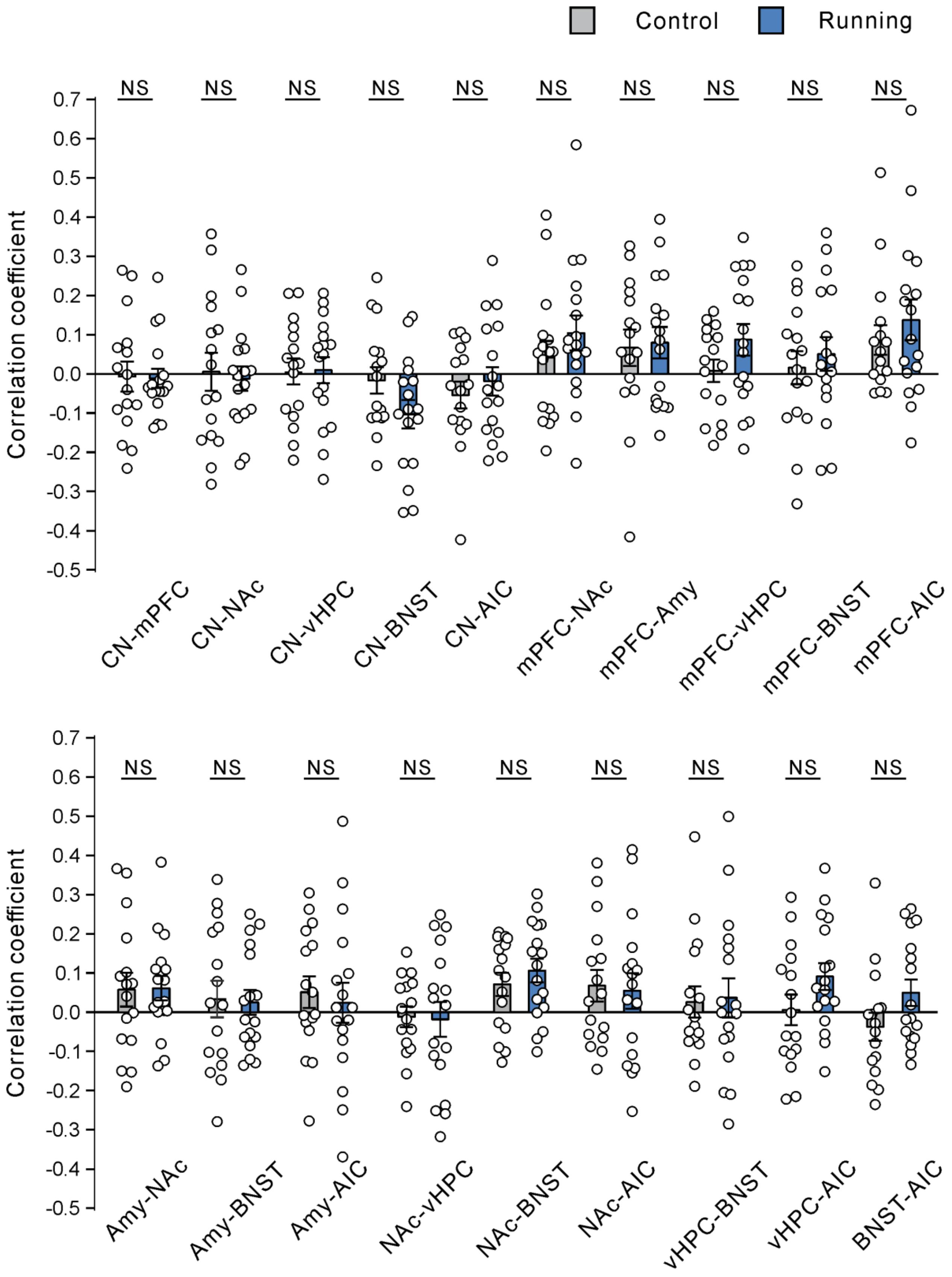

Control
Running
NS
Correlation coefficient
0.7
0.6
0.5
0.4
0.3
0.2
0.1
0.0
-0.1
-0.2
-0.3
-0.4
-0.5
CN-mPFC
CN-NAc
CN-vHPC
CN-BNST
CN-AIC
mPFC-NAc
mPFC-Amy
mPFC-vHPC
mPFC-BNST
mPFC-AIC
Amy-NAc
Amy-BNST
Amy-AIC
NAc-vHPC
NAc-BNST
NAc-AIC
vHPC-BNST
vHPC-AIC
BNST-AIC

Figure S4. Effect of rotarod running on functional connectivity between different brain regions, related to Figure 3

Statistics of the functional connectivity in the rat brain of control (grey, *n* = 16 rats) and constant rotarod running (10 rpm, blue, *n* = 17 rats) groups. Amy, amygdala; AIC, anterior insular cortex; BNST, bed nucleus of the stria terminalis; CN, cerebellar nuclei; mPFC, medial prefrontal cortex; NAc, nucleus accumbens; vHPC, ventral hippocampus.

Data are mean ± SEM. Unpaired t test. NS, not significant. For statistics, see Table S1.

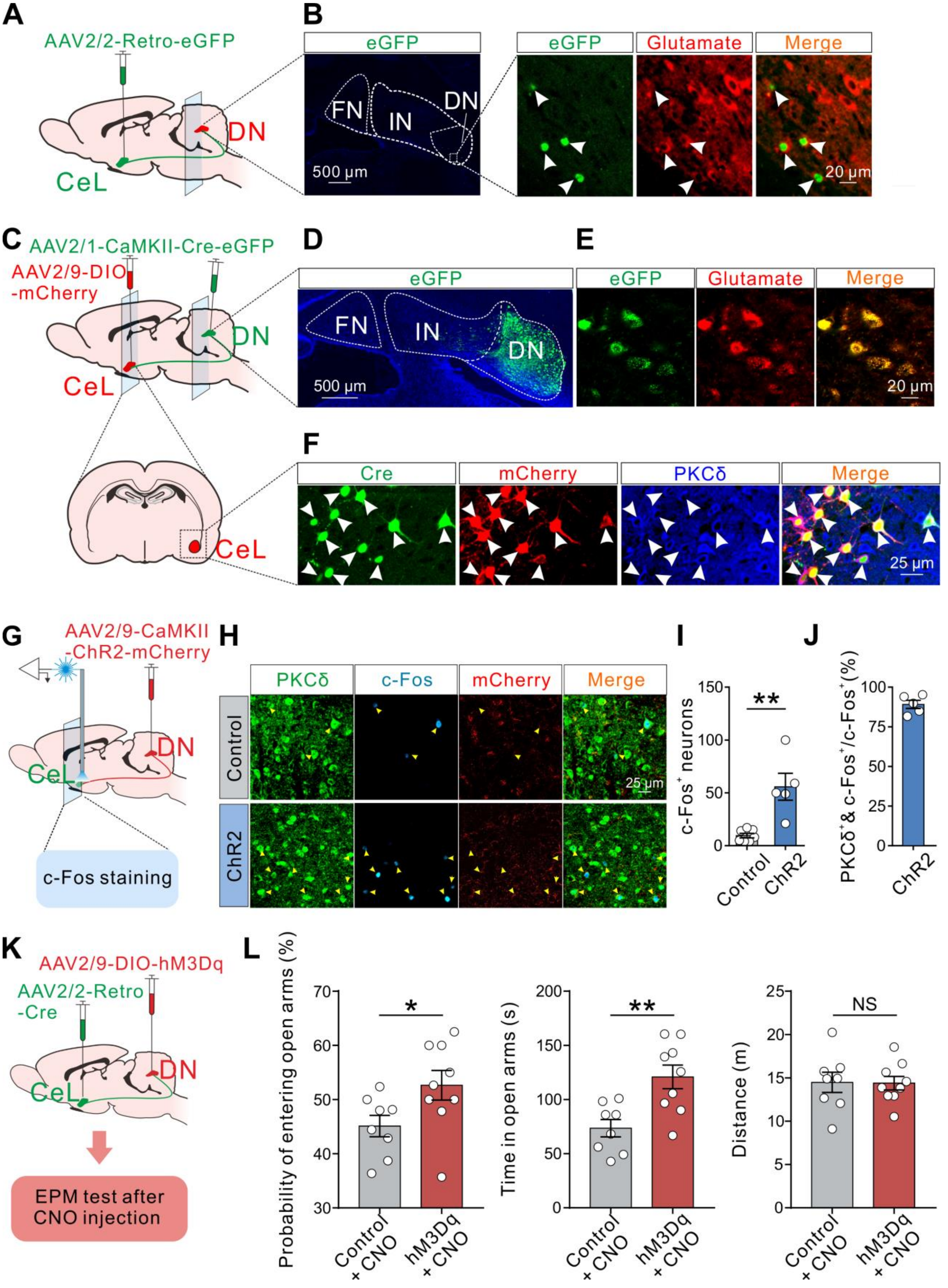
A
AAV2/2-Retro-eGFP
DN
CeL
B
eGFP
FN
IN
DN
500 μm
eGFP
Glutamate
Merge
20 μm
C
AAV2/1-CaMKII-Cre-eGFP
AAV2/9-DIO
-mCherry
DN
CeL
CeL
D
eGFP
FN
IN
DN
500 μm
E
eGFP
Glutamate
Merge
20 μm
F
Cre
mCherry
PKCδ
Merge
25 μm
G
AAV2/9-CaMKII
-ChR2-mCherry
DN
CeL
c-Fos staining
H
PKCδ
c-Fos
mCherry
Merge
Control
ChR2
25 μm
I
c-Fos⁺ neurons
150
100
50
0
**
Control
ChR2
J
PKCδ⁺& c-Fos⁺/c-Fos⁺(%)
100
75
50
25
0
ChR2
K
AAV2/9-DIO-hM3Dq
AAV2/2-Retro
-Cre
DN
CeL
EPM test after
CNO injection
L
Probability of entering open arms (%)
70
60
50
40
30
*
Control + CNO
hM3Dq + CNO
Time in open arms (s)
200
150
100
50
0
**
Control + CNO
hM3Dq + CNO
Distance (m)
25
20
15
10
5
0
NS
Control + CNO
hM3Dq + CNO

Figure S5. Glutamatergic neurons in DN project directly to PKCδ-positive neurons in CeL and their activation reduces anxiety-like behaviors, related to Figure 3

(A) Schematic of Retro-eGFP virus infusion in CeL.

(B) Confocal images showing retrogradely labeled DN^{CeL} neurons (eGFP) are glutamate immune-positive (red).

(C) Schematic of trans-monosynaptic anterograde virus AAV1-CaMKII-Cre-eGFP and Cre-dependent virus (mCherry) infusions in DN and CeL, respectively.

(D) A coronal image showing the microinjection site of trans-monosynaptic anterograde viral tracer AAV2/1-CaMKII-Cre-eGFP in DN.

(E) Confocal images of neurons that were transfected with the virus AAV2/1-CaMKII-Cre-eGFP showing co-localized glutamate-positive signals (red).

(F) Confocal images of CeL neurons that received direct monosynaptic projections from DN (double positive for Cre and mCherry) showing co-localized PKCδ-positive signals (blue).

(G) Schematic of intra-DN microinjection of AAV-CaMKII-ChR2 and c-Fos staining in CeL after opto-activation of DN-CeL glutamatergic terminals expressing ChR2.

(H) Confocal image of immunofluorescence labeling for PKCδ (green), c-Fos (cyan), and mCherry (red) in CeL with and without opto-genetic activation of DN-CeL glutamatergic terminals. Yellow arrowheads indicate the $PKC\delta^+$ CeL neurons expressing c-Fos.

(I) Statistics of the c-Fos expressing CeL neurons in control ($n = 7$ rats) and ChR2 (opto-activation) group ($n = 5$ rats).

(J) Proportions of $PKC\delta^+$ neurons expressing c-Fos in all of the c-Fos^+ CeL neurons ($n = 5$ rats).

(K and L) Chemogenetic activation of the DN^{CeL} glutamatergic neurons with Cre-dependent hM3Dq and CNO reduced anxiety-like behaviors in the elevated plus maze (EPM), whereas it did not affect locomotor activity ($n = 8$ rats for control + CNO; $n = 9$ rats for hM3Dq + CNO).

Data are mean ± SEM. Unpaired t test for (I) and (J). $*P < 0.05$; $**P < 0.01$; NS, not significant. For statistics, see Table S1.

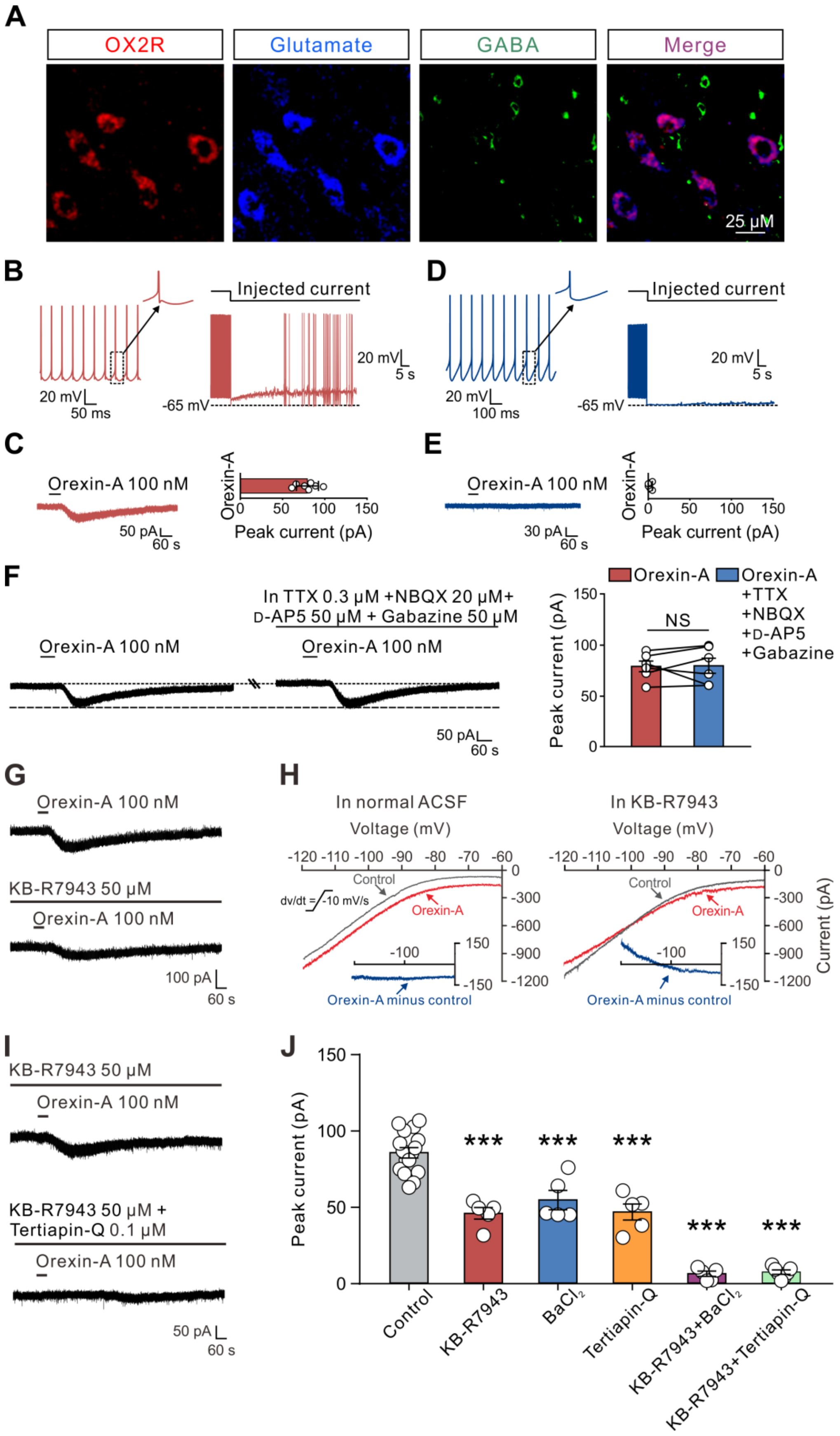
A
OX2R
Glutamate
GABA
Merge
25 μM
B
Injected current
20 mV
50 ms
-65 mV
20 mV
5 s
D
Injected current
20 mV
100 ms
-65 mV
20 mV
5 s
C
Orexin-A 100 nM
50 pA
60 s
Orexin-A
0
50
100
150
Peak current (pA)
E
Orexin-A 100 nM
30 pA
60 s
Orexin-A
0
50
100
150
Peak current (pA)
F
Orexin-A 100 nM
In TTX 0.3 μM +NBQX 20 μM+
D-AP5 50 μM + Gabazine 50 μM
Orexin-A 100 nM
50 pA
60 s
Orexin-A
Orexin-A +TTX +NBQX +D-AP5 +Gabazine
NS
Peak current (pA)
0
50
100
150
G
Orexin-A 100 nM
KB-R7943 50 μM
Orexin-A 100 nM
100 pA
60 s
H
In normal ACSF
Voltage (mV)
-120 -110 -100 -90 -80 -70 -60
0
-300
-600
-900
-1200
Control
dv/dt = -10 mV/s
Orexin-A
-100
150
-150
Orexin-A minus control
In KB-R7943
Voltage (mV)
-120 -110 -100 -90 -80 -70 -60
0
-300
-600
-900
-1200
Control
Orexin-A
-100
150
-150
Orexin-A minus control
Current (pA)
I
KB-R7943 50 μM
Orexin-A 100 nM
KB-R7943 50 μM +
Tertiapin-Q 0.1 μM
Orexin-A 100 nM
50 pA
60 s
J
Peak current (pA)
150
100
50
0
***
***
***
***
***
Control
KB-R7943
BaCl₂
Tertiapin-Q
KB-R7943+BaCl₂
KB-R7943+Tertiapin-Q

Figure S6. Orexin excites glutamatergic rather than GABAergic neurons in DN via activation of Na^+/Ca^{2+} Exchanger (NCX) and closure of inward rectifier K^+ channels, related to Figure 6

(A) Triple immunoreactivity of orexin 2 receptor (OX2R, red), glutamate (blue), and GABA (green) in DN, indicating a selective expression of OX2R in DN glutamatergic projection neurons.

(B) The DN glutamatergic projection neurons had a complex waveform of afterpotentials, composed of a fast afterhyperpolarization (AHP), an afterdepolarization, and then a slow AHP (left). When we injected a continuous intracellular hyperpolarizing current (upper right), the firing shifted from a tonic to a bursting pattern.

(C) Orexin-A elicited an inward current in glutamatergic projection neurons (n = 7 cells from 7 rats) in the DN.

(D) DN GABAergic neurons had a relatively simple afterpotential waveform with only one AHP included (left), and they stopped firing when we injected a continuous intracellular hyperpolarizing current (right).

(E) Orexin-A had no significant effect on GABAergic neurons (n = 5 cells from 5 rats) in DN.

(F) Combined application of TTX (selective voltage-gated sodium channel blocker), NBQX and D-AP5 (blockers for AMPA and NMDA receptors, respectively) as well as Gabazine (selective $GABA_A$ receptor antagonist) did not abolish the orexin-induced inward current in DN glutamatergic neurons (n = 6 cells from 6 rats), indicating a direct postsynaptic effect of orexin.

(G) KB-R7943, a selective blocker of NCX, partly blocked the orexin-A-elicited inward current in DN neurons.

(H) The *I*-*V* relationship of orexin-A-induced current in normal ACSF (left) differed from that in ACSF containing KB-R7943 (right). The orexin-A-induced current corresponds to the subtraction of the control current from the current recorded during the orexin-A application. Note that in the presence of KB-R7943, the orexin-A-induced current showed an outward rectification and reversed at a potential of -100 mV, which is near the calculated E_K, indicating orexin blocked the inward rectifier K^+ channels.

(I) KB-R7943 and Tertiapin-Q, a selective blocker for inward rectifier K^+ channels, nearly totally blocked the orexin-A-elicited inward current on DN neurons.

(J) Statistics of the orexin-A-induced inward current in DN neurons in the presence of control ACSF (*n* = 16 cells from 16 rats), KB-R7943 (*n* = 5 cells from 5 rats), $BaCl_2$ (a broad spectrum inhibitor of K^+ channels; *n* = 5 cells from 5 rats), Tertiapin-Q (*n* = 5 cells from 5 rats), KB-R7943 + $BaCl_2$ (*n* = 5 cells from 5 rats), or KB-R7943 + Tertiapin-Q (*n* = 7 cells from 7 rats).

Data are mean ± SEM. Paired t test for (F) and One-way ANOVA for (J). ***$P < 0.001$; NS, not significant. For statistics, see Table S1.

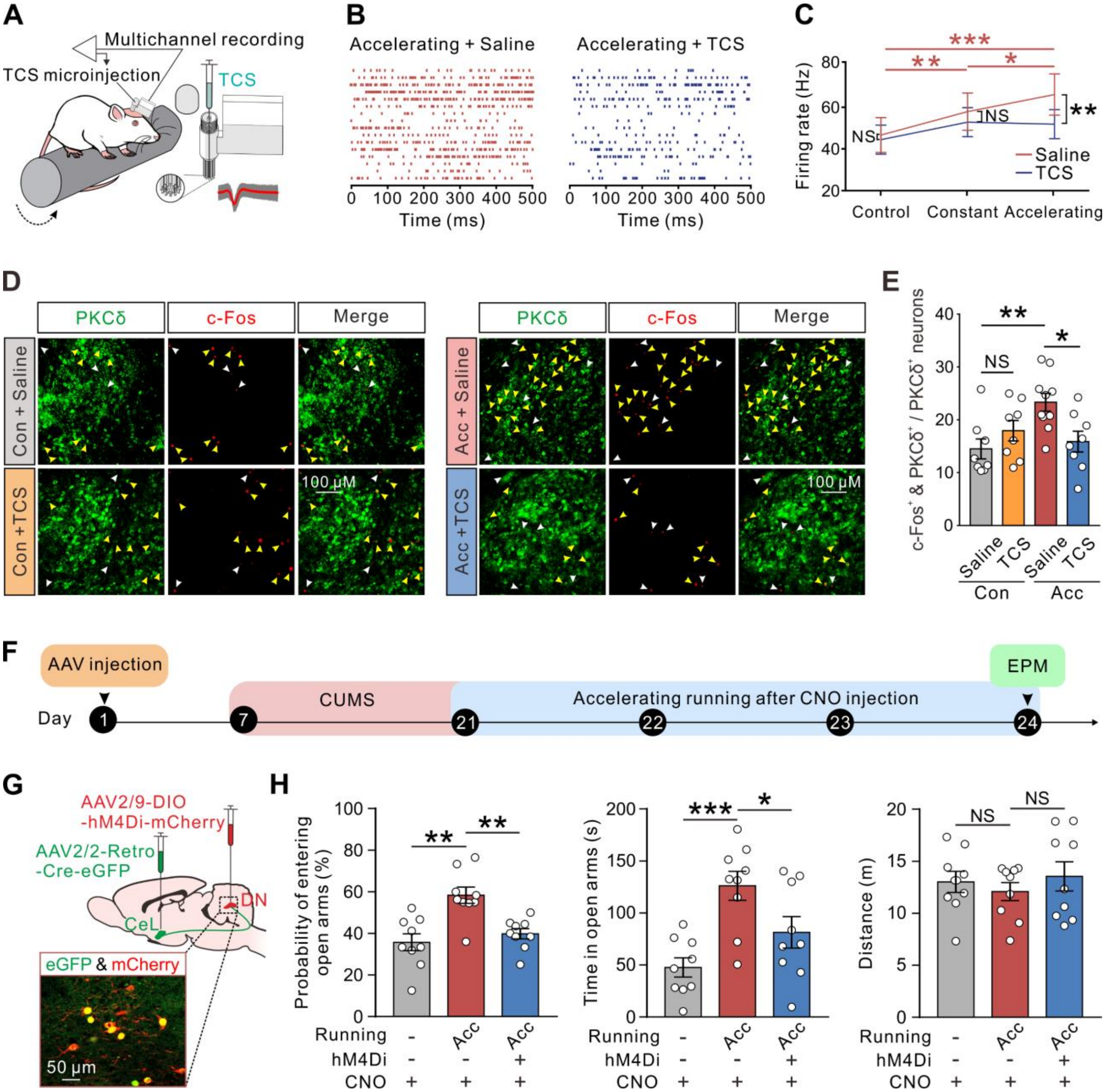

Figure S7. Challenge movement recruits cerebellar orexinergic afferent inputs to drive DN-CeL circuit and promote stress-induced anxiety, related to Figure 6

(A-C) Microinjection of selective orexin 2 receptor antagonist TCS-OX2-29 (TCS) into DN abolished the increase in firing rates of DN neurons induced by accelerating (acceleration of 0.2 rpm/s) rather than constant (10 rpm) rotarod running (*n* = 16 cells from 5 rats).

(D) Double immunoreactivity of PKCδ (green) and c-Fos (red) in CeL of rats that have been subjected to a rotarod test running at a constant or accelerating speed following microinjection of saline or TCS in DN. Yellow arrowheads indicate the activated PKCδ$^+$ neurons, whereas white arrowheads indicate the activated PKCδ$^-$ neurons.

(E) TCS had a significant inhibitory impact on c-Fos expression in CeL PKCδ$^+$ neurons in the accelerating rotarod condition only (n = 8 rats for constant (con) + saline; n = 8 rats for constant + TCS; n = 10 rats for accelerating (acc) + saline; n = 8 rats for accelerating + TCS).

(F and G) Scheme of AAV injections in CeL and DN, CUMS, CNO injection, accelerating running, and elevated plus maze test (EPM).

(H) Chemoinhibition of DN^{CeL} neurons suppressed the anxiolytic effects of accelerating rotarod running in CUMS rats (n = 9 rats for each group).

Data are mean ± SEM. RM two-way ANOVA for (C) and unpaired t test for (H). Two-way ANOVA for (E). *$P < 0.05$; **$P < 0.01$; ***$P < 0.001$. NS, not significant. For statistics, see Table S1.